Hox genes limit germ cell formation in the short germ insect *Gryllus bimaculatus*

Austen A. Barnett[a,1,2], Taro Nakamura[a,2,3], and Cassandra G. Extavour[a,b,4]

[a]Department of Organismic and Evolutionary Biology, Harvard University, Cambridge, MA 02138; and [b]Department of Molecular and Cellular Biology, Harvard University, Cambridge, MA 02138

Edited by Claude Desplan, New York University, New York, NY, and approved June 21, 2019 (received for review September 20, 2018)

Hox genes are conserved transcription factor-encoding genes that specify the identity of body regions in bilaterally symmetrical animals. In the cricket *Gryllus bimaculatus*, a member of the hemimetabolous insect group Orthoptera, the induction of a subset of mesodermal cells to form the primordial germ cells (PGCs) is restricted to the second through the fourth abdominal segments (A2 to A4). In numerous insect species, the Hox genes *Sex-combs reduced* (*Scr*), *Antennapedia* (*Antp*), *Ultrabithorax* (*Ubx*), and *abdominal-A* (*abd-A*) jointly regulate the identities of middle and posterior body segments, suggesting that these genes may restrict PGC formation to specific abdominal segments in *G. bimaculatus*. Here we show that reducing transcript levels of some or all of these Hox genes results in supernumerary and/or ectopic PGCs, either individually or in segment-specific combinations, suggesting that the role of these Hox genes is to limit PGC development with respect to their number, segmental location, or both. These data provide evidence of a role for this ancient group of genes in PGC development.

Hox | *Gryllus bimaculatus* | insect | evo-devo | germ cells

The Hox genes are an ancient family of transcription factor-encoding genes that play a conserved role in specifying the body regions of bilaterally symmetrical animals during development (reviewed in ref. 1). In arthropods, Hox genes act to specify the distinct identities of different body segments (reviewed in ref. 2), with mutations in Hox genes usually resulting in switches of segmental type called "homeotic transformations" (reviewed in ref. 3). We previously showed that in the cricket *Gryllus bimaculatus*, which belongs to the hemimetabolous insect order Orthoptera, the primordial germ cells (PGCs) form from the mesoderm of the second to the fourth abdominal segments (A2 to A4) (4) via a bone morphogenetic protein (BMP)-dependent mechanism (5). Given that BMP activity is not limited to the segments where PGCs form and develop, but rather is present in the dorsal regions of all body segments (5), these data suggested that some additional unidentified factor or factors must ensure that PGCs form in the appropriate segments. As Hox genes play a conserved role in establishing segmental identity, here we test the hypothesis that Hox genes contribute to regulating PGC development in A2 to A4.

Data implicating Hox genes in embryonic germ line development in other animal taxa are scarce. In the mouse *Mus musculus*, as in *G. bimaculatus*, PGCs are established via BMP signals that activate the transcription factor Blimp-1 (5–7). Mouse embryonic cells that take on PGC fate repress the Hox genes *Hoxa1* and *Hoxb1* via activity of the BMP-activated transcription factor Blimp-1 (7–9). This has been interpreted as reflecting the loss of somatic differentiation programs that is associated with adopting PGC fate. Repression of Hox genes during differentiation of human induced pluripotent stem cells into in vitro-derived PGCs (10) is consistent with the hypothesis that Hox gene expression and stable PGC fate within the same cells are mutually exclusive. In a system where germ cells are specified by inductive signals from neighboring cells, the degree or robustness of the PGC differentiation response may be influenced by the degree of concomitant Hox gene knockdown. Indeed, it was recently reported that, among mouse embryonic cells expressing PGC markers, there are some cells that also express hematopoietic markers, including at least one Hox gene (11). One interpretation of these observations is that those putative PGCs that respond to inductive signals by expressing lower levels of germ cell markers may still be prone to express some somatic markers. Thus, it may be that decreased levels, rather than total absence of expression, of somatic markers like Hox genes can facilitate the acquisition of PGC fate.

The relevance of Hox gene function to PGC fate is further exemplified by documented roles for Hox genes in the development of somatic gonad tissue. A role for HoxD genes in patterning and elongation of the external genitalia in mice has long been recognized (12–15), and HoxA genes are required for the correct development and function of elements of the female reproductive system that are derived from the Müllerian ducts, including the uterus and endometrium (16–19). However, the functions of Hox genes known to be expressed in the genital ridges, the precursors to the gonads (see, for example, ref. 20), has received less attention.

In contrast to *G. bimaculatus*, in the model insect *Drosophila melanogaster* PGCs form early in development (21, 22), long before the activation of the Hox genes that establish the identities of the body segments (23–26). Following gastrulation, the PGCs migrate toward the somatic gonad precursors (reviewed in ref. 27), which develop from the mesoderm of embryonic abdominal parasegments 10–12 (28). The Hox genes *abdominal-A* (*abd-A*) and *Abdominal-B* (*Abd-B*) are necessary for the formation of the gonad precursors, which is independent of PGC specification.

Significance

Hox genes are necessary for the proper placement of organs along animal body axes. In insects, Hox genes are used in a "code" of overlapping expression domains to specify body segments. We previously showed that, in the cricket *Gryllus bimaculatus*, germ cells are specified exclusively in the second through the fourth abdominal segments. Given the role of Hox genes in establishing segmental identity in insects, we tested the hypothesis that Hox genes control the segment-specific development of germ cells in crickets. We found that a subset of Hox genes limit germ cell development in the PGC-bearing segments. These data suggest a role for Hox genes in regulating germ cell placement.

Author contributions: C.G.E. designed research; A.A.B. and T.N. performed research; A.A.B., T.N., and C.G.E. analyzed data; and A.A.B. and C.G.E. wrote the paper.

The authors declare no conflict of interest.

This article is a PNAS Direct Submission.

[1]Present address: Department of Natural Sciences, DeSales University, Center Valley, PA 18034.

[2]A.A.B. and T.N. contributed equally to this work.

[3]Present address: Division of Evolutionary Developmental Biology, National Institute for Basic Biology, 444-8585 Okazaki, Japan.

[4]To whom correspondence may be addressed. Email: extavour@oeb.harvard.edu.

This article contains supporting information online at www.pnas.org/lookup/suppl/doi:10.1073/pnas.1816024116/-/DCSupplemental.

Published online July 25, 2019.

Specifically, *abd-A* establishes anterior gonad fates, and *abd-A* and *Abd-B* act in concert to establish the posterior gonad fates (28–31). In addition, in adult male *D. melanogaster*, *Abd-B* is required for correct function of the accessory gland (32), which is a component of the reproductive system that regulates the female response to mating (33). Moreover, this Hox gene is also required to maintain the identity of both germ line and somatic stem cells in the adult testis (34–37). However, these somatic and postembryonic functions of *Abd-B* do not affect embryonic PGC establishment in *D. melanogaster*, which takes place much earlier in development.

Across insects, the Hox genes *Sex-combs reduced* (*Scr*), *Antennapedia* (*Antp*), *Ultrabithorax* (*Ubx*), and *abdominal-A* (*abd-A*) have a conserved role in establishing the thoracic and abdominal segments during embryogenesis (reviewed in ref. 2). To explore the role of these Hox genes in the development of *G. bimaculatus* PGCs, we used embryonic RNAi (eRNAi) to repress the function of each of these genes individually and also in combination. We found that these Hox genes act to limit PGC formation in specific segments of the abdomen. Reminiscent of their combinatorial action in specifying other aspects of segment identity, including ectodermal patterning and appendage differentiation, these data suggest that specific combinations of Hox genes may also be needed for appropriate numbers of PGCs to develop and/or for them to occupy the correct segments. These data demonstrate a role for these highly conserved and ancient genes in limiting germ line development in an animal, and provide evidence for an additional embryonic role of Hox genes outside of establishing anterior–posterior segmental identity in an insect.

Results and Discussion

G. bimaculatus PGCs emerge from the lateral mesoderm of abdominal segments A2 to A4 during embryonic stage 5 (38) and come to form clusters within the mesoderm of either one or both hemisegments (i.e., the left or right halves of the segment) in embryonic stages 8 and 9 (4). Four Hox genes—*Scr* (*Gb-Scr*), *Antp* (*Gb-Antp*), *Ubx* (*Gb-Ubx*), and *abd-A* (*Gb-abd-A*) (*SI Appendix*, Figs. S1 and S2)— were previously reported (39, 40) to be expressed in the abdomen, including segments A2 to A4, at embryonic stage 5 (38) of *G. bimaculatus* embryogenesis, which is when germ cells are first detectable by molecular [enrichment of a number of gene products including Gb-Piwi protein (4)] and morphological [high nuclear-to-cytoplasmic ratio, loose chromatin compaction (4, 41, 42)] criteria. These expression data suggested that these four Hox genes could potentially be involved in early stages of PGC specification or development.

To investigate whether these posterior Hox genes were expressed at a time and place that could enable them to regulate development of PGCs following their initial specification, we performed in situ hybridization during embryonic stages 7 and 8 (38), the stages during which PGCs are proliferating and forming distinct clusters in each hemisegment (4). As previously described (39, 40), we found that the expression of these Hox genes exhibited spatial collinearity in the ectoderm from gnathal to abdominal segments in wild-type embryos at stage 8, a stage when all segments have been defined and are morphologically distinct (Fig. 1 and *SI Appendix*, Fig. S3). Because PGCs arise from the abdominal mesoderm, we asked whether these Hox genes were also expressed in the mesoderm. *Gb-Scr*, *Gb-Antp*, and *Gb-abd-A* transcripts were expressed in the mesodermal cells of the abdominal segments (Fig. 1 *B*, *C*, *E*, *G*, *H*, and *J*), whereas *Gb-Ubx* transcripts were not detected above background levels in the dorsal mesodermal cells of A2 to A10, but rather appeared to be restricted to the ectoderm in these segments (Fig. 1 *D* and *I*).

To determine whether the mesodermally expressed Hox genes were also expressed in PGCs, we conducted codetection of Piwi protein, a PGC marker in *G. bimaculatus* (4), and Hox gene transcripts. We detected *Gb-Scr*, *Gb-Antp*, and *Gb-abd-A* transcripts in mesodermal cells adjacent to PGCs at stages 7–8.5, but transcripts were undetectable or at very low levels in the PGCs themselves (Fig. 1 *B′*, *C′*, *E′*, *G′*, *H′*, and *J′*). *Gb-Ubx* expression

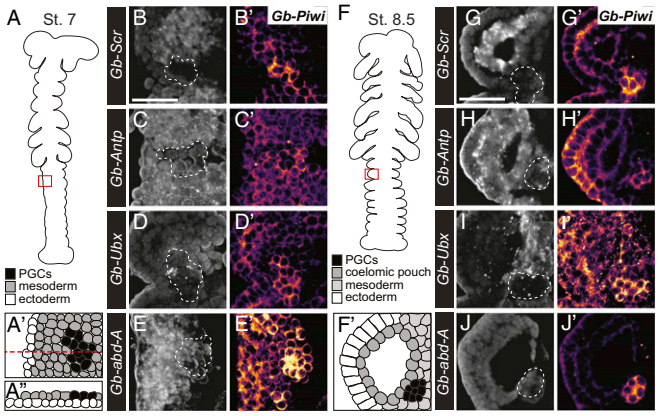

Fig. 1. Posterior Hox gene expression adjacent to but absent from *G. bimaculatus* PGCs. (*A* and *F*) Schematic illustration of whole embryos at the embryonic stages (St.) (38) used for expression analysis. Red rectangles in *A* and *F* show enlarged areas in *A′* and *B*–*E′* and in *F′* and *G*–*J′*, respectively. (*A′* and *F′*) schematics of dorsal views of areas contained within red rectangles in *A* and *F* showing spatial relationships between mesoderm (gray), coelomic pouch mesoderm (dark gray), ectoderm (white), and PGCs (black). (*A′′*) Schematic of orthogonal section through the plane indicated with the red dotted line in *A′*, dorsal side up, showing spatial relationship between ectoderm (white: ventral) and mesoderm (gray: dorsal). (*B*–*J*) In situ hybridization for *Gb-Scr*, *Gb-Antp*, *Gb-Ubx*, and *Gb-abd-A* expression in the third abdominal segment (A3) at St. 7 (*B*–*E*) and St. 8.5 (*G*–*J*) of wild-type embryos. (*B′*–*J′*) Costaining with Gb-Piwi protein (yellow: high levels; purple: low levels) in abdominal segment A3. (*B* and *G*) Expression of *Gb-Scr* is enriched in the abdominal mesoderm and undetectable above background levels in the ectoderm. (*B′* and *G′*) Costaining with Gb-Piwi protein reveals *Gb-Scr* expression is undetectable in PGCs. (*C* and *H*) *Gb-Antp* expression is detected in abdominal mesoderm and ectoderm. (*C′* and *H′*) *Gb-Antp* transcript is undetectable in *G. bimaculatus* PGCs at St. 7 and at very low levels at St. 8.5. (*D* and *I*) Weak *Gb-Ubx* expression is observed in the ventral mesoderm of A3. (*D′* and *I′*) PGCs do not express detectable *Gb-Ubx*. (*E* and *J*) High *Gb-abd-A* expression is detected in the A3 ectoderm and mesoderm. (*E′* and *J′*) PGCs display lower expression levels of *Gb-abd-A* than the adjacent mesoderm. [Scale bars, 100 μm in *B* (applies to *B*–*E′*) and *G* (applies to *G*–*J′*).]

was also undetectable in the PGCs at these stages (Fig. 1 *D* and *I*). Taken together, these results suggest that, as in mice, *G. bimaculatus* Hox gene transcription is active in somatic cells adjacent to PGCs at this stage, but is repressed or inactive within PGCs (7–9).

Given their expression in cells in close proximity to PGCs, we hypothesized that these Hox genes might play a role in PGC development. To test this hypothesis, we used eRNAi to abrogate the activity of one or more of these Hox genes during *G. bimaculatus* embryogenesis (*SI Appendix*, Table S1) and assessed the effect on PGC number and segmental position. Specifically, we compared the PGC number per hemisegment and per embryo, as well as the presence or absence of PGC clusters in each hemisegment, to controls (*SI Appendix*, Tables S2–S7). Our previous observations of hundreds of wild-type embryos have shown that, by embryonic stages 8 and 9, usually three or four of the A2 to A4 hemisegments, and, less commonly, fewer than three or more than four of these hemisegments, are populated by clusters of PGCs (4, 5). We thus examined embryos of embryonic stages 8 and 9 for this analysis, as these are the earliest stages at which PGCs can be reliably quantified (5, 6).

eRNAi against *Gb-Scr* efficiently depleted *Gb-Scr* transcripts as assessed by qPCR (*SI Appendix*, Fig. S4 *A* and *B*), although this was not accompanied by homeotic transformation of gnathal appendages to a thoracic identity ($n = 36$; Fig. 2*L*), as is often observed upon *Scr* knockdown in other insects (e.g., refs. 43 and 44). *Gb-Scr* eRNAi did, however, result in a statistically significant increase in PGC number as well as a significantly higher proportion of segments bearing PGC clusters in A2 to A4 relative

to controls (Fig. 2 *A*, *B*, *F*, and *G*). Furthermore, the total number of PGCs per embryo increased significantly relative to controls (Fig. 2*K*).

eRNAi against *Gb-Antp*, similarly to the *Gb-Scr* eRNAi treatment, did not result in a homeotic phenotype ($n = 14$; Fig. 2*L*). However, our qPCR results showed that this treatment was also sufficient to reduce *Gb-Antp* transcripts by 4 d after egg laying (AEL), the time at which we scored PGCs (*SI Appendix*, Fig. S4*B*). *Gb-Antp* eRNAi significantly increased the proportion of segments bearing PGC clusters in A1 to A4 and also increased PGC number in A2 (Fig. 2 *C* and *H*) and overall (Fig. 2*K*). Thus, loss of *Gb-Antp* resulted both in additional PGCs in the correct segments, as did loss of *Gb-Scr*, and also in ectopic PGCs in A1.

Gb-Ubx eRNAi resulted in a number of clear somatic homeotic phenotypes that were consistent with *Ubx* knockdowns in other insects (45–48). Specifically, we observed the transformation

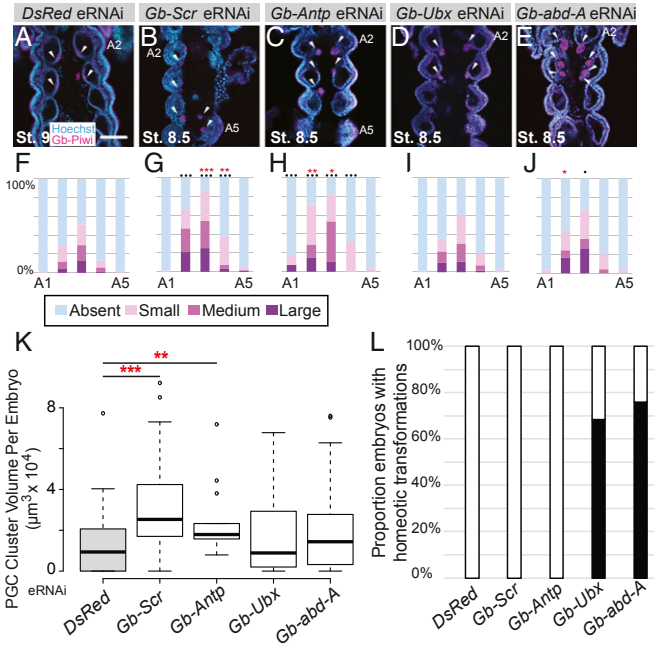

Fig. 2. eRNAi of *Gb-Scr*, *Gb-Antp*, and *Gb-abd-A* increases PGC number. (*A*–*E*) Confocal images of the A2–A5 of a representative embryo from each knockdown condition as well as the control condition (*DsRed* eRNAi). Gb-Piwi (magenta) marks PGC clusters (arrowheads) (4). The second abdominal segment (A2) is labeled in each panel. Anterior is up. (Scale bar, 100 μm.) (*F*–*J*) PGC cluster quantifications of each eRNAi treatment (*G*–*J*) compared with (*F*) *DsRed* controls. Blue: absent (0 μm^3, 0 PGCs); pink: small (<5,000 μm^3, 1–5 PGCs); magenta: medium (5,000–10,000 μm^3, 6–20 PGCs); purple: large (>10,000 μm^3, >20 PGCs). Sample sizes are $n = 82$, 36, 14, 41, and 25 embryos, and $n = 164$, 72, 28, 82, and 50 hemisegments scored for *F*–*J*, respectively. Red asterisks denote significant size differences of PGC clusters in that segment compared with controls. Black dots denote significant differences in presence/absence of PGC clusters compared with controls. Hemisegments were scored separately for the presence/absence and number of PGCs since in wild-type embryos a given segment may have PGCs in only one of the two hemisegments that comprise a segment (4, 5). (*K*) Box plot showing the distribution of total PGC volumes per embryo in each knockdown condition and the control condition (gray). Red asterisks denote significance levels resulting from a Mann–Whitney test. The whiskers extend to data points that are 1.5 times above the interquartile range away from the first or third quartile. The black lines represent the medians. Sample sizes are $n =$ 82, 36, 14, 41, and 25 embryos for each condition from left to right. (*L*) A 100% stacked bar chart showing the proportion of eRNAi embryos displaying homeotic phenotypes. St.: embryonic stage (38). Sample sizes are $n = 82$, 36, 14, 41, and 25 embryos for each condition from left to right. All *P* values for each test are listed in *SI Appendix*, Tables S2 and S4. */•$P < 0.05$, **$P < 0.01$, ***/•••$P < 0.001$.

of A1 appendages (pleuropodia) toward ectopic walking legs ($n =$ 28/41; Fig. 2*L* and *SI Appendix*, Figs. S5*B*, S6 *B* and *F*, and S7*A*), supported by expression of the appendage marker *Distal-less* (*Dll*) (49) (*SI Appendix*, Fig. S6*B*) and reduced expression of the *G. bimaculatus* ortholog of *tramtrack* (*ttk*), a gene that shows enriched expression in pleuropodia (*SI Appendix*, Fig. S6*F*). Accordingly, qPCR analysis indicated that *Gb-Ubx* transcripts were effectively reduced by the RNAi treatment (*SI Appendix*, Fig. S4 *A* and *B*). However, *Gb-Ubx* eRNAi did not significantly affect PGC number, or the numbers of PGC clusters, in any segment, or overall, relative to controls (Fig. 2 *D*, *I*, and *K*). Thus, we suggest that *Gb-Ubx* alone plays no or a minimal role in PGC development in this cricket.

eRNAi targeting *Gb-abd-A* transcripts resulted in ectopic appendages throughout all abdominal segments ($n = 19/25$; Fig. 2*L* and *SI Appendix*, Figs. S5*C*, S6 *C* and *G*, and S7*B*). These ectopic outgrowths expressed *Dll* (*SI Appendix*, Fig. S6*C*), but not *ttk* (*SI Appendix*, Fig. S6*G*), and were consistent with outgrowths observed in *abd-A* knockdowns in other insects (45, 50–53). qPCR confirmed a decrease in *Gb-abd-A* transcripts following the eRNAi treatment (*SI Appendix*, Fig. S4 *A* and *B*). *Gb-abd-A* eRNAi increased both PGC number in A2 and the proportion of hemisegments bearing PGC clusters in A3 (Fig. 2 *E*, *J*, and *K*). Together, the results of these single Hox gene knockdowns suggest that *Gb-Scr* and *Gb-abd-A* repress mesodermal transformation to PGCs in A2 to A3, and that *Gb-Antp* represses PGC formation in A1 to A4.

In arthropods, Hox genes often work in concert to either activate or repress transcriptional targets (reviewed in ref. 2). Moreover, Hox genes often cross-regulate each other's expression in multiple developmental contexts (e.g., ref. 54). Therefore, we explored the possibility that the aforementioned Hox genes could be acting together in the context of PGC specification. We predicted that, if a combination of Hox genes worked together to modulate PGC formation, a double knockdown of these genes might result in unique PGC defects relative to the defects observed in the single knockdowns discussed above. To test this prediction, we systematically injected embryos with equal amounts of dsRNA targeting each pairwise combination of these posterior *G. bimaculatus* Hox genes (*SI Appendix*, Table S1). Consistent with our prediction, for each double knockdown combination tested, we indeed found that the resulting PGC phenotypes could not be simply deduced from the component single-knockdown phenotypes.

Unexpectedly, all double eRNAi treatments that involved *Gb-Scr* dsRNA as a partner resulted in embryonic lethality 1 d after injection (*SI Appendix*, Table S1). We therefore could not study its interaction with the other Hox genes, and instead focused on the remaining three possible pairwise double-knockdown combinations. The first of these, eRNAi simultaneously targeting *Gb-Antp* and *Gb-Ubx*, resulted in the same embryonic homeotic transformation as *Gb-Ubx* single knockdowns (i.e., an ectopic fourth leg on A1, $n = 27/31$; *SI Appendix*, Figs. S5*D* and S7*C*). This double knockdown also resulted in an increase in the presence of PGCs in A2 to A5, as well as an increase in the number of PGCs in segments A2 to A4, and overall, compared with controls (Fig. 3 *A*, *D*, and *E*). Comparing these results to the *Gb-Ubx* and *Gb-Antp* single knockdowns, the overall PGC increase induced by the double knockdown (Fig. 3*D*) was not significantly different from that induced by the *Gb-Antp* knockdown alone (Fig. 2*K*), suggesting that *Gb-Antp* acts without *Gb-Ubx* to repress PGC formation in A2 to A4. However, the reduction in A1 PGC number in the double knockdown (Fig. 3*A*) relative to *Gb-Antp* alone (Fig. 2*H*) suggests that *Gb-Antp* may act to repress a PGC formation-promoting function of *Gb-Ubx* in A1. Furthermore, the presence of significantly more PGC clusters in A5 in the double knockdown (Fig. 3 *A* and *E*) relative to both single knockdowns (Fig. 2 *H* and *I*) also suggests that these genes act together to repress PGC formation in A5.

RNAi simultaneously targeting *Gb-Ubx* and *Gb-abd-A* resulted in embryos with ectopic legs throughout the abdomen ($n = 8/14$;

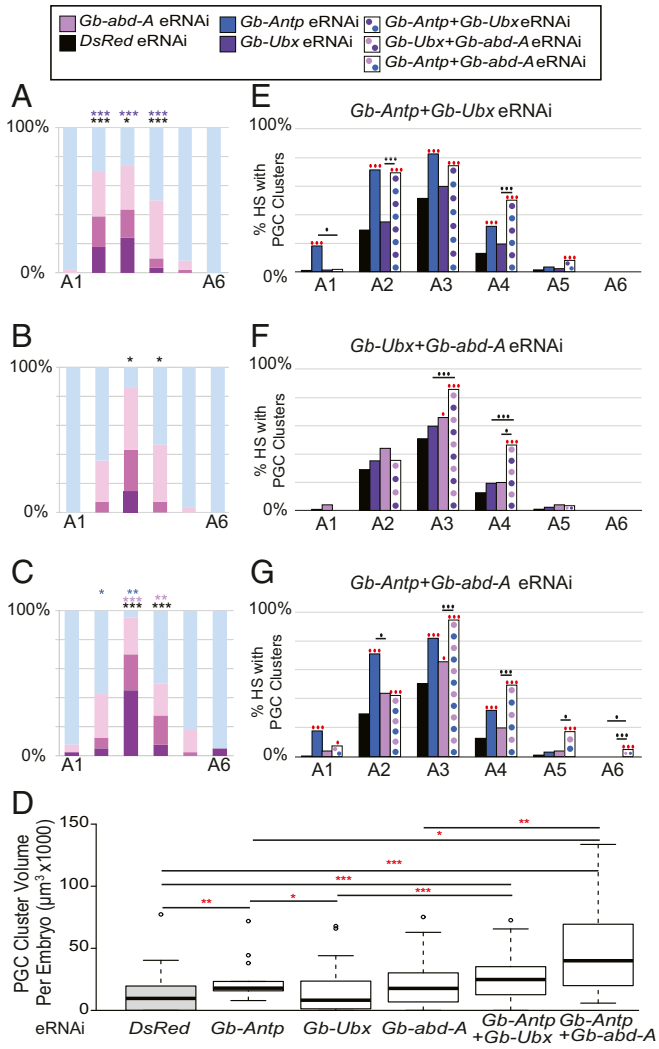

Fig. 3. Double eRNAi reveals synergistic effects of Hox repression on germ cells. (*A–C*) PGC cluster quantifications of each eRNAi treatment (double RNAi treatment indicated by label above adjacent panels *E–G*, respectively). Blue: absent (0 µm^3, 0 PGCs); pink: small (<5,000 µm^3, 1–5 PGCs); magenta: medium (5,000–10,000 µm^3, 6–20 PGCs); purple: (large >10,000 µm^3, >20 PGCs). Sample sizes are n = 31, 14, and 20 embryos, and n = 62, 28, and 40 hemisegments scored for *A–C*, respectively. Asterisks denote significant size differences from *DsRed* controls (Fig. 2*F*) and single eRNAi treatments (Fig. 2 *G–J*) in that segment; asterisk colors indicate comparisons to *DsRed* (black), *Gb-Antp* eRNAi (dark blue), *Gb-abd-A* eRNAi (light purple), or *Gb-Ubx* eRNAi (dark purple). See *SI Appendix*, Tables S3 and S6, for statistical values. (*D*) Box plot showing the distribution of total PGC volumes per embryo in each knockdown condition and the control condition (gray) except for *Gb-Ubx+Gb-abd-A* eRNAi, which displayed no significant total PGC differences in total. Red asterisks denote significance levels in PGC number resulting from a Mann–Whitney test for differences in PGC number. The whiskers extend to data points that are 1.5 times above the interquartile range away from the first or third quartile. The black lines represent the medians. Sample sizes are n = 82, 14, 41, 25, 31, and 20 embryos for each condition from left to right. See *SI Appendix*, Tables S2, S3, and S6, for statistical values. (*E–G*) Bar plots showing the proportion of hemisegments (HS) containing PGC clusters in single vs. double eRNAi treatments. Sample sizes are n = 31, 14, and 20 embryos, and n = 62, 28, and 40 hemisegments scored for *E–G*, respectively. The dots represent significance levels testing for the presence/absence of PGC clusters using a Fisher's Exact or χ^2 test; red: compared with *DsRed* control; black: comparisons between single and double eRNAi conditions. See *SI Appendix*, Tables S4, S5, and S7, for statistical values. $^{*/\bullet}P < 0.05$, $^{**}P < 0.01$, $^{***/\bullet\bullet\bullet}P < 0.001$.

SI Appendix, Figs. S5*E* and S7*D*), exhibiting a similar phenotype to other studied insects (45, 52). These embryos also have significantly more PGC clusters in A3 and A4 compared with controls, as well as an increase in total PGC number in A4 (Fig. 3 *B* and *F*). However, the overall increase in PGCs per embryo compared with controls was not statistically significant (*SI Appendix*, Table S3). Comparing these results to the *Gb-Ubx* and *Gb-abd-A* single knockdowns suggests that *Gb-abd-A* alone is negatively regulating PGC formation in A3, and that both *Gb-Ubx* and *Gb-abd-A* act together to limit PGC formation in A4 (compare Fig. 2 *I* and *J* with Fig. 3*B*).

The effect of eRNAi of *Gb-Antp* and *Gb-abd-A* together on PGCs was striking: A1 to A6 contained significantly more PGC clusters than in controls (Fig. 3 *C*, *D*, and *G*), and there were significantly more PGCs in A3 to A4 and overall. Comparing this double knockdown to the single *Gb-Antp* and *Gb-abd-A* knockdowns revealed that the PGC increase caused by *Gb-Antp* eRNAi alone (Fig. 2*H*) was slightly suppressed in A2 (Fig. 3*C*), suggesting a potential role of *Gb-Antp* in repressing *Gb-abd-A*'s ability to promote PGC formation in A2. Furthermore, this double knockdown provided evidence that *Gb-Antp* and *Gb-abd-A* act together to suppress PGC development in A3, A6, and overall (Fig. 3 *D* and *G*).

Together, our results are consistent with a role of Hox genes in suppressing the formation of PGCs in *G. bimaculatus* abdominal segments (Fig. 4). We propose that this role is at least partially independent of the role of Hox genes in encoding segmental identity, as the embryonic somatic homeotic phenotypes obtained upon Hox gene RNAi do not always correlate with PGC positioning defects. For example, when we repress *Gb-abd-A* via eRNAi, A2 to A3 bear pleuropodia-like appendages (*SI Appendix*, Figs. S5*C* and S6*C*). In wild-type embryos, the pleuropodia are on A1, and thus we might expect that, in this eRNAi condition, A2 to A3 are transformed to an A1 identity. As the A1 segment generally lacks PGCs (4, 5), we should not observe PGCs in these segments in *Gb-abd-A* eRNAi-injected embryos. However, instead we see an increase in PGCs in these segments in this condition (Fig. 2*J*). In another example, *Gb-Ubx+Gb-abd-A* eRNAi embryos bear ectopic leg-like structures on all abdominal segments (*SI Appendix*, Fig. S5*E*). Given that *G. bimaculatus*

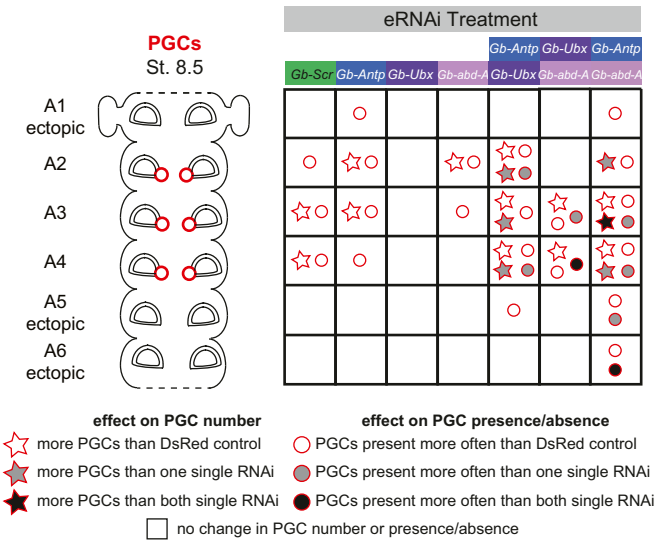

Fig. 4. Hypothesis: Combinatorial action of Hox genes regulates segmental positions of PGCs. Summary of the eRNAi PGC number and presence/absence phenotypes. (*Left*) In wild-type embryos, PGC clusters (red circles) form in segments A2 to A4 (4). (*Right*) Statistically significant changes in PGC number (star symbols) and/or statistically significant changes in the presence of PGC clusters (circle symbols) are labeled for each of the segments A1 to A6 in each of the single and double eRNAi conditions tested here.

wild-type embryos lack PGCs on their leg-bearing (thoracic) segments (4), we might expect an absence of Hox genes in A2 to A4 in this eRNAi condition. However, instead we see an increase in the presence of PGCs in these segments (Fig. 3*B*). Furthermore, we note that the *Gb-Scr* and *Gb-Antp* single eRNAi embryos, although they lacked the somatic homeotic appendage transformations reported in loss-of-function conditions of these genes in other insects (Fig. 2*L*) (43, 44), nevertheless had significantly more PGCs than controls (Fig. 2*K*). We hypothesize that PGC number may be more sensitive than appendage differentiation to the levels of expression of these genes. However, we cannot rule out the possibility that off-target RNAi effects, or interactions of our targeted genes with other, unknown genes, account for our observation of supernumerary PGCs despite the apparent absence of somatic homeotic transformation.

In addition, we note that even in conditions where Hox gene RNAi results in a significant increase in total PGC number, including the appearance of ectopic PGCs, PGCs are still largely restricted to segments A2 to A4, and most abdominal segments remain free of PGCs, as in wild type. This suggests that additional, still-unknown mechanisms must act to prevent PGC formation outside of A2 to A4. It is therefore possible that the role of these Hox genes in PGC development is a generally repressive role that acts in concert with or in addition to whatever factors provide the spatial information that restricts germ cells to the A2 to A4 segments.

The single or combinatorial use of Hox genes to pattern organs outside of the "Hox code" that confers regional identity along primary anterior–posterior or proximal–distal axes of animals has been reported in other taxa. In insects, such nonaxial Hox roles have also been previously described, such as those needed for the positioning of the bacteriomes in the seed bug *Nysius plebeius* (51), the formation of the lantern organ in the firefly *Photuris* (*sp*.) (55), and the differentiation of a specific accessory gland cell type in male fruit flies (32). Our results provide an example of Hox genes being used to coordinate cell-type specification, namely the specification of PGCs. In this context, Hox genes may contribute to correct gonad positioning in the context of the body plan, or simply to appropriate gonad function, by ensuring that an appropriate number of PGCs are available to populate the primordial gonad.

Our results suggest that Hox genes may play an indirect role in PGC specification. As has been suggested in the case of mouse PGC specification (7, 8, 56), down-regulation of Hox genes may suppress somatic fate, permitting or facilitating adoption of PGC fate by BMP-responding cells. Alternatively, Hox genes may act in the somatic cells adjacent to PGCs to negatively regulate PGC fate, thus limiting one or both of the number of cells that can adopt PGC fate, or the position where PGCs emerge in the abdominal segments. The stage in development at which PGCs are reliably quantifiable (4 d AEL) is nearly 2 d after their initial specification (2.5 d AEL). Thus, changes in PGC number or placement that are observed at 4 d AEL could be the result of changes in any or all of their initial specification at 2.5 d AEL, subsequent proliferation, putative apoptosis, maintenance, or short-range migration to the correct segmental locations (4). Our eRNAi experiments likely disrupt transcript levels before and during this entire phase of PGC development. As a result we cannot definitively address which of the processes described above may require Hox gene input.

These caveats notwithstanding, one possible role for these Hox genes in A2 to A4 may be to regulate an appropriate number of PGCs in the area where the gonad must form. An alternative, but not mutually exclusive, possibility is that Hox gene expression suppresses PGC fate in somatic gonad precursors such that loss of Hox gene expression results in an expansion of the PGC population at the expense of somatic gonad precursor cells. *G. bimaculatus* PGCs do not undergo long-range migration (5), and the cells of the somatic gonad primordia are thought to lie within A2 to A4 (4). As a first step toward testing these hypotheses, we asked if *G. bimaculatus* orthologs of *Six4* and *eyes absent* (*eya*), gonad primordia markers used in *Drosophila* (57, 58), could identify putative somatic gonad precursors in *G. bimaculatus*. However, in situ hybridization did not show enhanced expression of either gene in cells adjacent to PGCs in A2 to A4 (*SI Appendix*, Fig. S8). These data suggest that either the gonad primordia are specified at later stages, or that these genes are not used to specify gonad primordia in *G. bimaculatus*. As a somatic gonad precursor marker is currently unavailable for *G. bimaculatus*, at this time we cannot determine whether Hox genes regulate both PGC and somatic gonad cell fate independently, or in a coordinated manner. Further work will thus be needed to determine whether the increase in PGCs induced by many of the Hox eRNAi conditions is at the expense of mesoderm that would have been fated to be somatic gonadal cells in wild-type embryos in this cricket.

Finally, we note that, although we detect expression of these Hox genes in the regions containing PGCs (Fig. 1 and *SI Appendix*, Fig. S3) (39), given the systemic nature of the RNAi technique that we have employed here, we cannot formally rule out the hypothesis that Hox genes affect PGCs indirectly through action in some other body part or extraembryonic territory where Hox genes are also expressed. *Gb-Scr*, *Gb-Antp*, and *Gb-Ubx* are expressed in thoracic and abdominal segments both anterior and posterior to A2 to A4 during the time of PGC specification and cluster formation, as well as in gnathal segments in the case of *Gb-Scr* (refs. 39 and 40 and *SI Appendix*, Fig. S3). *Gb-abd-A* expression extends through all abdominal segments during this developmental window (refs. 39 and 40 and *SI Appendix*, Fig. S3). To our knowledge, extraembryonic expression of these Hox genes has not been reported to date. Although we consider it more likely that the Hox eRNAi-induced PGC effects that we have reported here are due to Hox gene activity in the specific segments where we observed these effects, we cannot eliminate the possibility of a long-distance, tissue-nonautonomous role for posterior Hox genes in PGC development.

As in other animals with discrete gonads, arthropod PGCs must meet with somatic gonad cells and end up in a specific location in the body to form a functional gonad. In arthropods, the location of the gonad, and often the location of PGCs when they first arise, is tied to specific body segments. In insects like *Drosophila*, where PGCs form much earlier than Hox gene activation and must migrate to the primordial gonad, the somatic gonad precursors rely on Hox genes to form in specific segments (28). In the beetle *Tenebrio molitor*, distinct PGC clusters form in many abdominal segments, and then coalesce into only those segments that will ultimately contain the gonads (59). In the firebrat *Thermobia domestica* and the stick insect *Carausius morosus*, PGCs are thought to originate as a long cluster spanning multiple segments before ultimately becoming confined to the gonads within specific segments (reviewed in ref. 60). Outside of insects, in the spider *Parasteatoda tepidariorum*, the germ cells also arise as clusters, which are situated in the opisthosomal segments 2–6 (61). Considering the functional genetic *G. bimaculatus* data presented here in the context of these data from various arthropods, we speculate that, in addition to their roles in segment identity specification, one or both of (a) assigning the PGC-bearing segments or (b) regulating the development of PGCs within the appropriate segments may be additional ancestral roles for Hox genes in arthropods.

Materials and Methods

All Hox genes were cloned using a previously published *G. bimaculatus* transcriptome (62). The predicted translations of the resulting sequences were subjected to phylogenetic analysis to corroborate orthology (*SI Appendix*, Fig. S2). Animal husbandry, eRNAi (*SI Appendix*, Table S1), embryonic staging, cloning and qPCR (*SI Appendix*, Table S8), in situ hybridizations and immunostainings, statistical tests, and PGC quantifications were performed as previously described (4–6, 38). See *SI Appendix* for detailed methods.

ACKNOWLEDGMENTS. We thank Dr. Taro Mito (University of Tokushima) for kindly allowing us access to draft genomic data for *G. bimaculatus*. We appreciate the comments of two anonymous reviewers that helped improve the manuscript. This work was supported by NSF award IOS-1257217 to (C.G.E).

1. S. M. Hrycaj, D. M. Wellik, Hox genes and evoution. *F1000Res.* **5**, 859 (2016).
2. C. L. Hughes, T. C. Kaufman, Hox genes and the evolution of the arthropod body plan. *Evol. Dev.* **4**, 459–499 (2002).
3. J. C. G. Hombría, B. Lovegrove, Beyond homeosis: HOX function in morphogenesis and organogenesis. *Differentiation* **71**, 461–476 (2003).
4. B. Ewen-Campen, S. Donoughe, D. N. Clarke, C. G. Extavour, Germ cell specification requires zygotic mechanisms rather than germ plasm in a basally branching insect. *Curr. Biol.* **23**, 835–842 (2013).
5. S. Donoughe *et al*., BMP signaling is required for the generation of primordial germ cells in an insect. *Proc. Natl. Acad. Sci. U.S.A.* **111**, 4133–4138 (2014).
6. T. Nakamura, C. G. Extavour, The transcriptional repressor Blimp-1 acts downstream of BMP signaling to generate primordial germ cells in the cricket *Gryllus bimaculatus*. *Development* **143**, 255–263 (2016).
7. Y. Ohinata *et al*., Blimp1 is a critical determinant of the germ cell lineage in mice. *Nature* **436**, 207–213 (2005).
8. M. Saitou, S. C. Barton, M. A. Surani, A molecular programme for the specification of germ cell fate in mice. *Nature* **418**, 293–300 (2002).
9. K. Kurimoto *et al*., Complex genome-wide transcription dynamics orchestrated by Blimp1 for the specification of the germ cell lineage in mice. *Genes Dev.* **22**, 1617–1635 (2008).
10. T. S. Park *et al*., Derivation of primordial germ cells from human embryonic and induced pluripotent stem cells is significantly improved by coculture with human fetal gonadal cells. *Stem Cells* **27**, 783–795 (2009).
11. M. L. Scaldaferri *et al*., Hematopoietic activity in putative mouse primordial germ cell populations. *Mech. Dev.* **136**, 53–63 (2015).
12. P. Dollé, D. Duboule, Two gene members of the murine HOX-5 complex show regional and cell-type specific expression in developing limbs and gonads. *EMBO J.* **8**, 1507–1515 (1989).
13. J. Zákány, C. Fromental-Ramain, X. Warot, D. Duboule, Regulation of number and size of digits by posterior Hox genes: A dose-dependent mechanism with potential evolutionary implications. *Proc. Natl. Acad. Sci. U.S.A.* **94**, 13695–13700 (1997).
14. J. Cobb, D. Duboule, Comparative analysis of genes downstream of the Hoxd cluster in developing digits and external genitalia. *Development* **132**, 3055–3067 (2005).
15. P. Dollé, J. C. Izpisúa-Belmonte, J. M. Brown, C. Tickle, D. Duboule, HOX-4 genes and the morphogenesis of mammalian genitalia. *Genes Dev.* **5**, 1767–7 (1991).
16. H. Du, H. S. Taylor, The role of Hox genes in female reproductive tract development, adult function, and fertility. *Cold Spring Harb. Perspect. Med.* **6**, a023002 (2015).
17. B. Xu *et al*., Regulation of endometrial receptivity by the highly expressed HOXA9, HOXA11 and HOXD10 HOX-class homeobox genes. *Hum. Reprod.* **29**, 781–790 (2014).
18. Y. Ma *et al*., Knockdown of Hoxa11 in vivo in the uterosacral ligament and uterus of mice results in altered collagen and matrix metalloproteinase activity. *Biol. Reprod.* **86**, 100 (2012).
19. A. B. Ekici *et al*., HOXA10 and HOXA13 sequence variations in human female genital malformations including congenital absence of the uterus and vagina. *Gene* **518**, 267–272 (2013).
20. S. J. Gaunt, P. L. Coletta, D. Pravtcheva, P. T. Sharpe, Mouse Hox-3.4: Homeobox sequence and embryonic expression patterns compared with other members of the Hox gene network. *Development* **109**, 329–339 (1990).
21. A. F. Huettner, The origin of the germ cells in *Drosophila melanogaster*. *J. Morphol.* **37**, 385–423 (1923).
22. R. Lehmann, Germ plasm biogenesis: An *oskar*-centric perspective. *Curr. Top. Dev. Biol.* **116**, 679–707 (2016).
23. M. E. Akam, A. Martinez-Arias, The distribution of *Ultrabithorax* transcripts in *Drosophila* embryos. *EMBO J.* **4**, 1689–1700 (1985).
24. M. Levine, E. Hafen, R. L. Garber, W. J. Gehring, Spatial distribution of Antennapedia transcripts during *Drosophila* development. *EMBO J.* **2**, 2037–2046 (1983).
25. A. Martinez-Arias, The *Antennapedia* gene is required and expressed in parasegments 4 and 5 of the *Drosophila* embryo. *EMBO J.* **5**, 135–141 (1986).
26. A. Martinez-Arias, P. W. Ingham, M. P. Scott, M. E. Akam, The spatial and temporal deployment of *Dfd* and *Scr* transcripts throughout development of *Drosophila*. *Development* **100**, 673–683 (1987).
27. A. C. Santos, R. Lehmann, Germ cell specification and migration in *Drosophila* and beyond. *Curr. Biol.* **14**, R578–R589 (2004).
28. M. Boyle, S. DiNardo, Specification, migration and assembly of the somatic cells of the *Drosophila* gonad. *Development* **121**, 1815–1825 (1995).
29. S. Greig, M. Akam, The role of homeotic genes in the specification of the *Drosophila* gonad. *Curr. Biol.* **5**, 1057–1062 (1995).
30. L. A. Moore, H. T. Broihier, M. Van Doren, L. B. Lunsford, R. Lehmann, Identification of genes controlling germ cell migration and embryonic gonad formation in *Drosophila*. *Development* **125**, 667–678 (1998).
31. V. Riechmann, K. P. Rehorn, R. Reuter, M. Leptin, The genetic control of the distinction between fat body and gonadal mesoderm in *Drosophila*. *Development* **125**, 713–723 (1998).
32. D. Gligorov, J. L. Sitnik, R. K. Maeda, M. F. Wolfner, F. Karch, A novel function for the Hox gene *Abd-B* in the male accessory gland regulates the long-term female postmating response in *Drosophila*. *PLoS Genet.* **9**, e1003395 (2013).
33. R. A. Leopold, The role of male accessory glands in insect reproduction. *Annu. Rev. Entomol.* **21**, 199–221 (1976).
34. S. Zhang *et al*., Repression of *Abd-B* by Polycomb is critical for cell identity maintenance in adult *Drosophila* testis. *Sci. Rep.* **7**, 5101 (2017).
35. J. R. Morillo Prado, X. Chen, M. T. Fuller, Polycomb group genes Psc and Su(z)2 maintain somatic stem cell identity and activity in *Drosophila*. *PLoS One* **7**, e52892 (2012).
36. F. Papagiannouli, L. Schardt, J. Grajcarek, N. Ha, I. Lohmann, The Hox gene *Abd-B* controls stem cell niche function in the *Drosophila* testis. *Dev. Cell* **28**, 189–202 (2014).
37. L. Schardt, J. J. Ander, I. Lohmann, F. Papagiannouli, Stage-specific control of niche positioning and integrity in the *Drosophila* testis. *Mech. Dev.* **138**, 336–348 (2015).
38. S. Donoughe, C. G. Extavour, Embryonic development of the cricket *Gryllus bimaculatus*. *Dev. Biol.* **411**, 140–156 (2016).
39. H. Zhang *et al*., Expression patterns of the homeotic genes *Scr*, *Antp*, *Ubx*, and *abd-A* during embryogenesis of the cricket *Gryllus bimaculatus*. *Gene Expr. Patterns* **5**, 491–502 (2005).
40. Y. Matsuoka *et al*., Short germ insects utilize both the ancestral and derived mode of Polycomb group-mediated epigenetic silencing of Hox genes. *Biol. Open* **4**, 702–709 (2015).
41. W. M. Wheeler, A contribution to insect morphology. *J. Morphol.* **8**, 1–161 (1893).
42. M. L. Roonwal, Studies on the embryology of the African migratory locust, *Locusta migratoria migratoides* Reiche and Frm. II. Organogeny. *Philos. Trans. R. Soc. Lond. B Biol. Sci.* **227**, 175–244 (1937).
43. C. L. Hughes, T. C. Kaufman, RNAi analysis of *Deformed, proboscipedia* and *Sex combs reduced* in the milkweed bug *Oncopeltus fasciatus*: Novel roles for Hox genes in the hemipteran head. *Development* **127**, 3683–3694 (2000).
44. S. Hrycaj, J. Chesebro, A. Popadić, Functional analysis of Scr during embryonic and post-embryonic development in the cockroach, *Periplaneta americana*. *Dev. Biol.* **341**, 324–334 (2010).
45. D. R. Angelini, P. Z. Liu, C. L. Hughes, T. C. Kaufman, Hox gene function and interaction in the milkweed bug *Oncopeltus fasciatus* (Hemiptera). *Dev. Biol.* **287**, 440–455 (2005).
46. R. L. Bennett, S. J. Brown, R. E. Denell, Molecular and genetic analysis of the *Tribolium Ultrabithorax* ortholog, Ultrathorax. *Dev. Genes Evol.* **209**, 608–619 (1999).
47. Z. Zheng, A. Khoo, D. Fambrough Jr, L. Garza, R. Booker, Homeotic gene expression in the wild-type and a homeotic mutant of the moth *Manduca sexta*. *Dev. Genes Evol.* **209**, 460–472 (1999).
48. A. Khila, E. Abouheif, L. Rowe, Evolution of a novel appendage ground plan in water striders is driven by changes in the Hox gene Ultrabithorax. *PLoS Genet.* **5**, e1000583 (2009).
49. G. Panganiban *et al*., The origin and evolution of animal appendages. *Proc. Natl. Acad. Sci. U.S.A.* **94**, 5162–5166 (1997).
50. E. Sánchez-Herrero, I. Guerrero, J. Sampedro, A. González-Reyes, Developmental consequences of unrestricted expression of the *abd-A* gene of *Drosophila*. *Mech. Dev.* **46**, 153–167 (1994).
51. Y. Matsuura, Y. Kikuchi, T. Miura, T. Fukatsu, *Ultrabithorax* is essential for bacteriocyte development. *Proc. Natl. Acad. Sci. U.S.A.* **112**, 9376–9381 (2015).
52. D. L. Lewis, M. DeCamillis, R. L. Bennett, Distinct roles of the homeotic genes Ubx and abd-A in beetle embryonic abdominal appendage development. *Proc. Natl. Acad. Sci. U.S.A.* **97**, 4504–4509 (2000).
53. J. J. Stuart, S. J. Brown, R. W. Beeman, R. E. Denell, The *Tribolium* homeotic gene Abdominal is homologous to *abdominal-A* of the *Drosophila* bithorax complex. *Development* **117**, 233–243 (1993).
54. D. F. Miller *et al*., Cross-regulation of Hox genes in the *Drosophila melanogaster* embryo. *Mech. Dev.* **102**, 3–16 (2001).
55. M. S. Stansbury, A. P. Moczek, The function of Hox and appendage-patterning genes in the development of an evolutionary novelty, the *Photuris* firefly lantern. *Proc. Biol. Sci.* **281**, 20133333 (2014).
56. K. Kurimoto, M. Yamaji, Y. Seki, M. Saitou, Specification of the germ cell lineage in mice: A process orchestrated by the PR-domain proteins, Blimp1 and Prdm14. *Cell Cycle* **7**, 3514–3518 (2008).
57. I. B. Clark, A. P. Jarman, D. J. Finnegan, Live imaging of *Drosophila* gonad formation reveals roles for *Six4* in regulating germline and somatic cell migration. *BMC Dev. Biol.* **7**, 52 (2007).
58. M. Boyle, N. Bonini, S. DiNardo, Expression and function of *clift* in the development of somatic gonadal precursors within the *Drosophila* mesoderm. *Development* **124**, 971–982 (1997).
59. S. L. Ullmann, The origin and structure of the mesoderm and the formation of the coelomic sacs in *Tenebrio molitor* L. (Insecta, Coleoptera). *Philos. Trans. R. Soc. Lond. B Biol. Sci.* **248**, 245–277 (1964).
60. M. Koch, B. Quast, T. Bartolomaeus, "Coeloms and nephridia in annelids and arthropods" in *Deep Metazoan Phylogeny: The Backbone of the Tree of Life*, J. W. Wägele, T. Bartolomaeus, Eds. (De Gruyter, Berlin, 2014), pp. 173–284.
61. E. E. Schwager, Y. Meng, C. G. Extavour, *vasa* and *piwi* are required for mitotic integrity in early embryogenesis in the spider *Parasteatoda tepidariorum*. *Dev. Biol.* **402**, 276–290 (2015).
62. V. Zeng *et al*., Developmental gene discovery in a hemimetabolous insect: *De novo* assembly and annotation of a transcriptome for the cricket *Gryllus bimaculatus*. *PLoS One* **8**, e61479 (2013).

PNAS
www.pnas.org

Supplementary Information for

Hox genes limit germ cell formation in the short germ insect *Gryllus bimaculatus*

Austen A. Barnett*, Taro Nakamura*, and Cassandra G. Extavour

Cassandra G. Extavour
Email: extavour@oeb.harvard.edu

* These authors contributed equally to this work.

This PDF file includes:

Supplementary Text
Supplementary Materials & Methods
Figs. S1 to S8
Tables S1 to S8
References for SI reference citations

Supplementary Text

Limitations of using systemic eRNAi data to infer involvement of widely expressed genes in specific developmental processes

When assessing the results of RNAi-based genetic perturbations in less-commonly employed model organisms like *G. bimaculatus*, it is important to acknowledge the ways in which our interpretations may be limited by the level of resolution possible with such experiments. In the case of this cricket, RNAi is systemic, and there are currently no tissue-specific or otherwise conditional knockdown methods available (1). For all functional genetic experiments described above, we injected dsRNA to trigger the RNAi response within the first few hours after egg laying (see Methods), and assessed transcript levels both at 2.5d AEL, when PGCs first begin to form (2), and also at 4d AEL, the time at which we scored PGC number and location (Fig. S4). We noted that in the case of single and double eRNAi experiments involving *Gb-Antp*, and for *Gb-abd-A* in the *Gb-Antp+Gb-abd-A* double eRNAi experiment, transcript levels appeared to increase temporarily at 2.5 d AEL (Fig. S4A,C) prior to their clear decrease by 4d AEL (Fig. S4B,D). This is an effect that we have observed in eRNAi experiments with other genes, and that we suspect may be an artifact of the presence of high levels of dsRNA that match the sequence of the target gene (3). In all other cases of both single and double knockdown experiments, however, as described above, target transcripts were always effectively reduced by at least 80% by 4d AEL (Fig. S4B,D). Moreover, we observed homeotic phenotypes in somatic tissues for *Gb-Ubx* and *Gb-abd-A* single eRNAi, and for *Gb-Ubx+Gb-Antp* and *Gb-Ubx+Gb-abd-A* double eRNAi experiments, that were consistent with conserved Hox gene roles across insects (Fig. S5). Taken together, these observations suggest that the somatic and PGC phenotypes reported here are due to abrogation of the target genes in each case.

Nevertheless, we attempted to address the additional possibility that off-target effects, cross-regulatory effects, or both might be contributing to these phenotypes. We therefore examined the transcript levels of all four Hox genes under study in each of the single and double eRNAi conditions. At 2.5d AEL, we observed that in all cases, at least one other Hox gene other than the target gene appeared to show changes in transcript levels (Fig. S4A,C). By 4d AEL, all four Hox genes had decreased transcript levels relative to controls (Fig. S4B,D). We considered the possibility that these results could be due to specific cross-regulatory effects between these Hox genes. However, this possibility is not strongly supported by our data: only two regulatory hypotheses are consistent with 2.5d AEL qPCR data from all experiments, namely, that *Gb-Ubx* positively regulates *Gb-Scr*, and that *Gb-abd-A* positively regulates *Gb-Ubx* (Fig. S4). Furthermore, neither of these putative regulatory interactions is consistent with previous reports that *Ubx* negatively regulates *Scr*, and that *abd-A* negatively regulates *Ubx*, in multiple developmental contexts (see for example 4, 5-9). We consider that off-target effects do not explain these observations well either, as transcript levels are different at the two developmental time points, and the transcript level responses seen with single eRNAi for a given gene are not always recapitulated in double eRNAi experiments involving the same gene. Moreover, the effects on PGCs and the somatic homeotic transformations were specific and different for each single and double knockdown

experiment, despite the fact that all four genes appear to have reduced transcript levels at the time of PGC scoring.

Taken together, we suggest that the most conservative interpretation of our data is that perturbation of one or more of these posterior Hox genes disrupts PGC development, resulting in extra and/or PGCs. A less conservative, alternative interpretation that aims to account for the fact that PGC phenotypes were different for each experiment, is that (1) modification of Hox gene activity earlier than 4d AEL is primarily responsible for the observed changes in PGC number and location; and (2) apparently altered levels of non-target Hox gene transcripts notwithstanding, in each single and double eRNAi experiment, specific reduction of the target transcript(s) is primarily responsible for the observed phenotypes. Since there are currently no suitable techniques available for *G. bimaculatus*, we cannot perform the spatially or temporally controlled knockdown experiments that would be needed to distinguish between these hypotheses. Indeed, to our knowledge, there have thus far been no quantitative approaches to studying Hox gene interactions in a non-*Drosophila* insect.

Supplementary Materials and Methods

Phylogenetic Analysis

Protein sequences of 119 annotated arthropod Hox gene (Fig. S1) and Distal-less (Dll) orthologues (for use as an outgroup) were retrieved from GenBank. These 119 sequences were used to make an alignment using MUSCLE (10) with eight iterations. The Smart Model Selection program (11) was used to find the best matrix for use in constructing the phylogeny (VT; AIC=164894.36226) and the best "decoration" (+G+I+F; AIC=164894.20896). This model was used with the resulting MUSCLE alignment to construct a maximum likelihood tree using PhyML (12). This resulted in a tree with a log likelihood of -81351.14064 (Fig. *S2*).

Quantitative PCR

Double stranded RNA (dsRNA) was injected as previously described (13) at 6 μg/μl for single eRNAi treatments, and at 3 μg/μl per dsRNA for double eRNAi treatments. Anterior abdominal segments A1-A5 were dissected from control or Hox gene eRNAi-treated embryos (n=5 per treatment for 2.5d and n=3 per treatment for 4d) using fine tungsten needles or fine forceps, and segments were pooled into single tubes. Total RNA was extracted using Trizol (Life Technologies) or RNeasy Mini Kit (Qiagen) following the manufacturer's directions. RNA pools were divided into two samples and each half was reverse transcribed to prepare cDNA using SuperScript III (Invitrogen). A no-reverse transcriptase control was performed in parallel for each sample. Each cDNA was divided into three replicate samples and used for qPCR. An MxP3005 machine (Stratagene) or a LightCycler 96 machine (Roche) was used for qPCR as previously described (3). Relative transcript ratios in the qPCR study were calculated from experiments performed in triplicate and are shown as mean±standard deviation in Fig. S4. The housekeeping gene *G. bimaculatus* β-*tubulin* was used as an internal control as previously described (3) . Primers used are listed in Table S8.

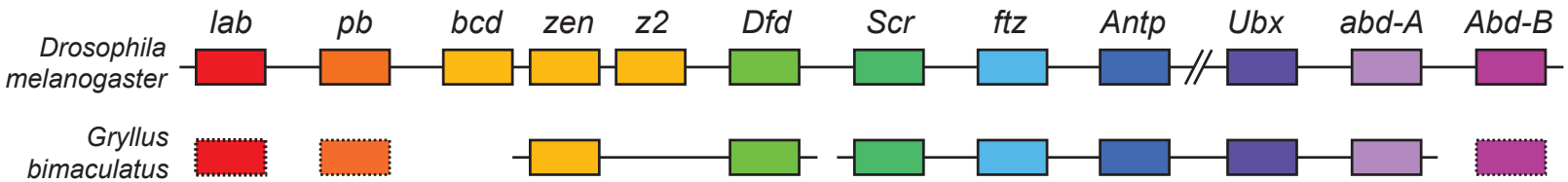

Fig. S1. Putative chromosomal arrangement of the *G. bimaculatus* Hox complex. Schematic representation of the Hox complexes of *D. melanogaster* and *G. bimaculatus*. Orthologous genes are shown as color-coded boxes. Dashed rectangle represents genes found in *G. bimaculatus* transcriptome databases but not mapping to the *G. bimaculatus* draft genome. Bar shows scaffold in *G. bimaculatus*; gaps indicate regions where scaffold information is unavailable. Double backslash in *D. melanogaster* cluster indicates the break between the Antennapedia complex and the Bithorax cluster complex. Illustration is not to scale.

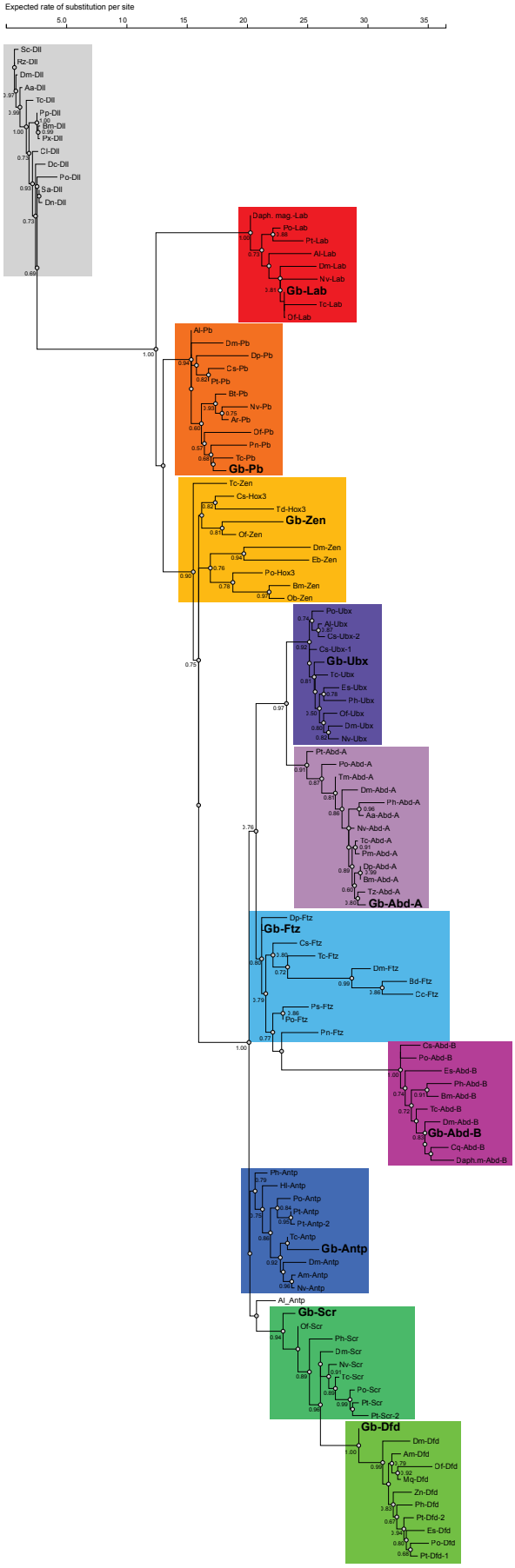
Expected rate of substitution per site
5.0
10
15
20
25
30
35
Sc-Dll
Rz-Dll
Dm-Dll
Aa-Dll
Tc-Dll
Pp-Dll
Bm-Dll
Px-Dll
Cl-Dll
Dc-Dll
Po-Dll
Sa-Dll
Dn-Dll
Daph. mag.-Lab
Po-Lab
Pt-Lab
Al-Lab
Dm-Lab
Nv-Lab
Gb-Lab
Tc-Lab
Of-Lab
Al-Pb
Dm-Pb
Dp-Pb
Cs-Pb
Pt-Pb
Bt-Pb
Nv-Pb
Ar-Pb
Of-Pb
Pn-Pb
Tc-Pb
Gb-Pb
Tc-Zen
Cs-Hox3
Td-Hox3
Gb-Zen
Of-Zen
Dm-Zen
Eb-Zen
Po-Hox3
Bm-Zen
Ob-Zen
Po-Ubx
Al-Ubx
Cs-Ubx-2
Cs-Ubx-1
Gb-Ubx
Tc-Ubx
Es-Ubx
Ph-Ubx
Of-Ubx
Dm-Ubx
Nv-Ubx
Pt-Abd-A
Po-Abd-A
Tm-Abd-A
Dm-Abd-A
Ph-Abd-A
Aa-Abd-A
Nv-Abd-A
Tc-Abd-A
Pm-Abd-A
Dp-Abd-A
Bm-Abd-A
Tz-Abd-A
Gb-Abd-A
Dp-Ftz
Gb-Ftz
Cs-Ftz
Tc-Ftz
Dm-Ftz
Bd-Ftz
Cc-Ftz
Ps-Ftz
Po-Ftz
Pn-Ftz
Cs-Abd-B
Po-Abd-B
Es-Abd-B
Ph-Abd-B
Bm-Abd-B
Tc-Abd-B
Dm-Abd-B
Gb-Abd-B
Cq-Abd-B
Daph.m-Abd-B
Ph-Antp
Hl-Antp
Po-Antp
Pt-Antp
Pt-Antp-2
Tc-Antp
Gb-Antp
Dm-Antp
Am-Antp
Nv-Antp
Al_Antp
Gb-Scr
Of-Scr
Ph-Scr
Dm-Scr
Nv-Scr
Tc-Scr
Po-Scr
Pt-Scr
Pt-Scr-2
Gb-Dfd
Dm-Dfd
Am-Dfd
Of-Dfd
Mq-Dfd
Zn-Dfd
Ph-Dfd
Pt-Dfd-2
Es-Dfd
Po-Dfd
Pt-Dfd-1

Fig. S2. Maximum likelihood phylogeny of all *G. bimaculatus* predicted Hox amino acid sequences and other arthropod Hox amino acid sequences. Orthologous Hox clades are boxed and color-coded as in Figure S1. Distal-less (Dll) protein sequences were used as an outgroup. All nodes with approximate likelihood ratio tests (SH-like) support values with a value greater than or equal to 0.50 are labeled with the support value above the node. The tree resulted from an alignment of 119 arthropod amino acid protein sequences retrieved from GenBank. Protein abbreviations are as follows: Abd-A, Abdominal-A; Abd-B, Abdominal-B; Antp, Antennapedia; Dfd, Deformed; Ftz, Fushi tarazu; Pb, Proboscipedia; Scr, Sex combs reduced; Ubx, Ultrabithorax; Zen, Zerknullt. All prefixes to these Hox proteins denote species names, as follows: Aa, *Aedes albopictus*; Al, *Archegozetes longisetosus*; Am, *Apis mellifera*; Ar, *Athalia rosae*; Bd, *Bacrocera dorsalis*; Bm, *Bombyx mori*; Bt, *Bombus terrestris*; Cc, *Ceratitis capitata*; Cl, *Cimex lectularis*; Cq, *Culex quinquefasciatus*; Cs, *Cupiennius salei*; Daph. mag., *Daphnia magna*; Dc, *Diaphorini citri*; Dm, *Drosophila melanogaster*; Dn, *Diuraphis noxia*; Dp, *Daphnia pulex*; Eb, *Episyrphus balteatus*; Es, *Endeis spinosa*; Gb, *Gryllus bimaculatus*; Hl, *Habropoda laboriosa*; Mq, *Melipona quadrifasciata*; Nv, *Nasonia vitripennis*; Ob, *Operophtera brumata*; Of, *Oncopeltus fasciatus*; Ph, *Parhyale hawaiiensis*; Pm, *Papilio machaon*; Pn, *Paracyclopina nana*; Po, *Phalangium opilio*; Ps, *Pedetontus saltator*; Pt, *Parasteatoda tepidariorum*; Px, *Plutella xylostella*; Rz, *Rhagoletis zephyria*; Sc, *Stomoxys calcitrans*; Tc, *Tribolium castaneum*; Td, *Thermobia domestica*; Tm, *Tenebrio molitor*; Tz, *Trachymyrmex zeteki*; Zn, *Zootermopsis nevadensis*.

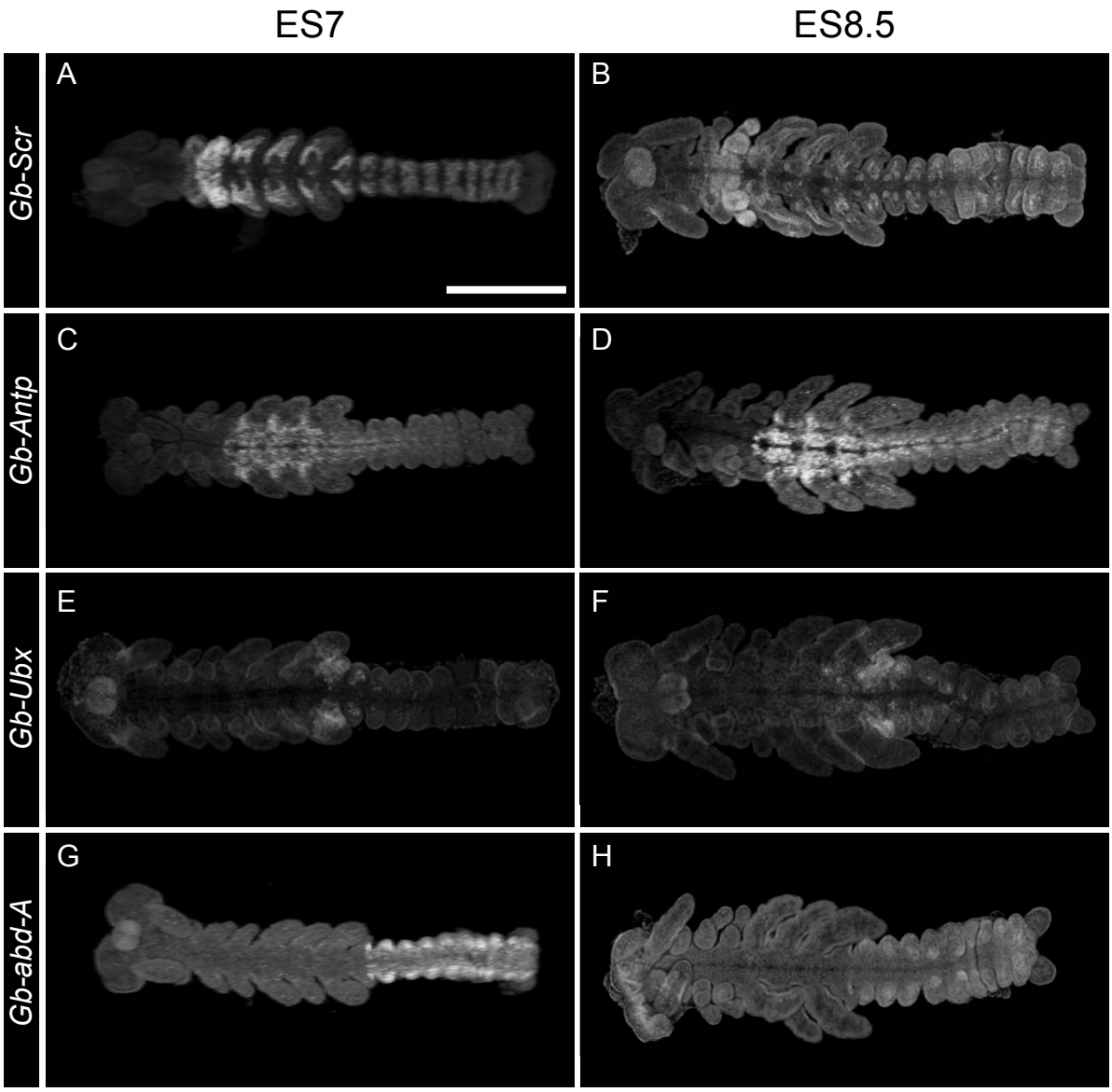

Fig. S3. Expression of *Gb-Scr*, *Gb-Antp*, *Gb-Ubx* and *Gb-abd-A* transcripts during *G. bimaculatus* development. Fluorescent *in situ* hybridization of wild type embryos at egg stage (ES) ES7 (A, C, E ,G) and ES8.5 (B, D, F, H). Egg staging as described in (14). Scale bar in (A) = 500 μm and applies to all panels.

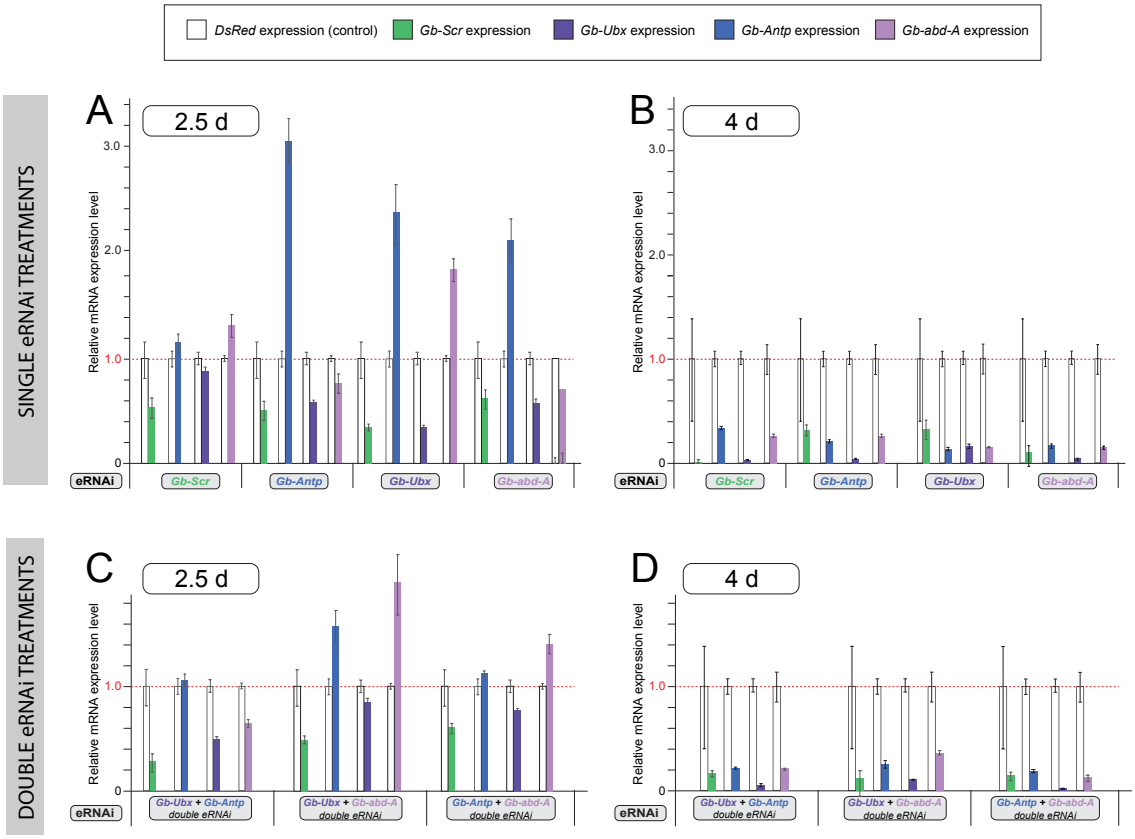

Fig. S4. Validation of eRNAi knockdown via qPCR. Quantitative PCR was conducted to evaluate the efficacy of eRNAi-mediated knockdown against Hox genes in embryos at 2.5 days (d) (A, C) and 4d (B. D) after egg laying (AEL). At 2.5d AEL, PGC formation begins and at 4d AEL, PGC clusters are formed (2). Bars show relative expression levels normalized to *Gb-beta-tubulin*. Error bars show standard deviation.

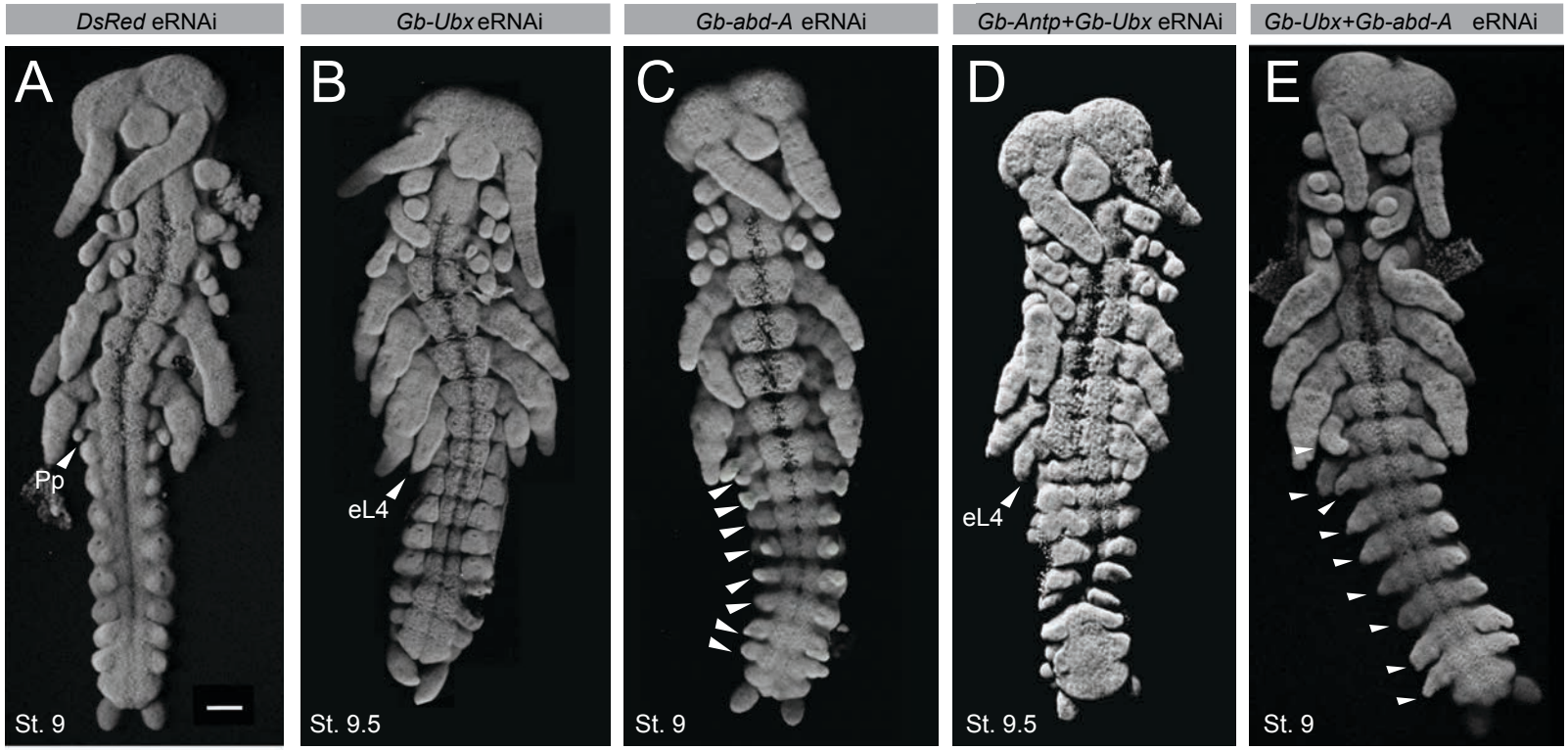

Fig. S5. Homeotic transformations resulting from Hox eRNAi. (A) Example of an embryonic stage (St.) St.9 *DsRed* eRNAi control embryo showing the wild-type morphology, with pleuropodia (Pp) on the first abdominal segment (A1). (B) *Gb-Ubx* eRNAi resulted in the transformation of the pleuropodia into ectopic legs (eL4) on A1. (C) *Gb-abd-A* eRNAi resulted in the formation of ectopic pleuropodia-like appendages (arrowheads) on segments A2-A9. (D) Double eRNAi targeting *Gb-Antp* and *Gb-Ubx* resulted in the formation of ectopic legs (eL4) on A1. (E) Double eRNAi targeting *Gb-Ubx* and *Gb-abd-A* resulted in leg-like appendages (arrowheads) forming on segments A1-A9. Scale bar in (A) = 100 μm and applies to all panels. All images are projections of optical confocal sections of embryos stained with Hoechst.

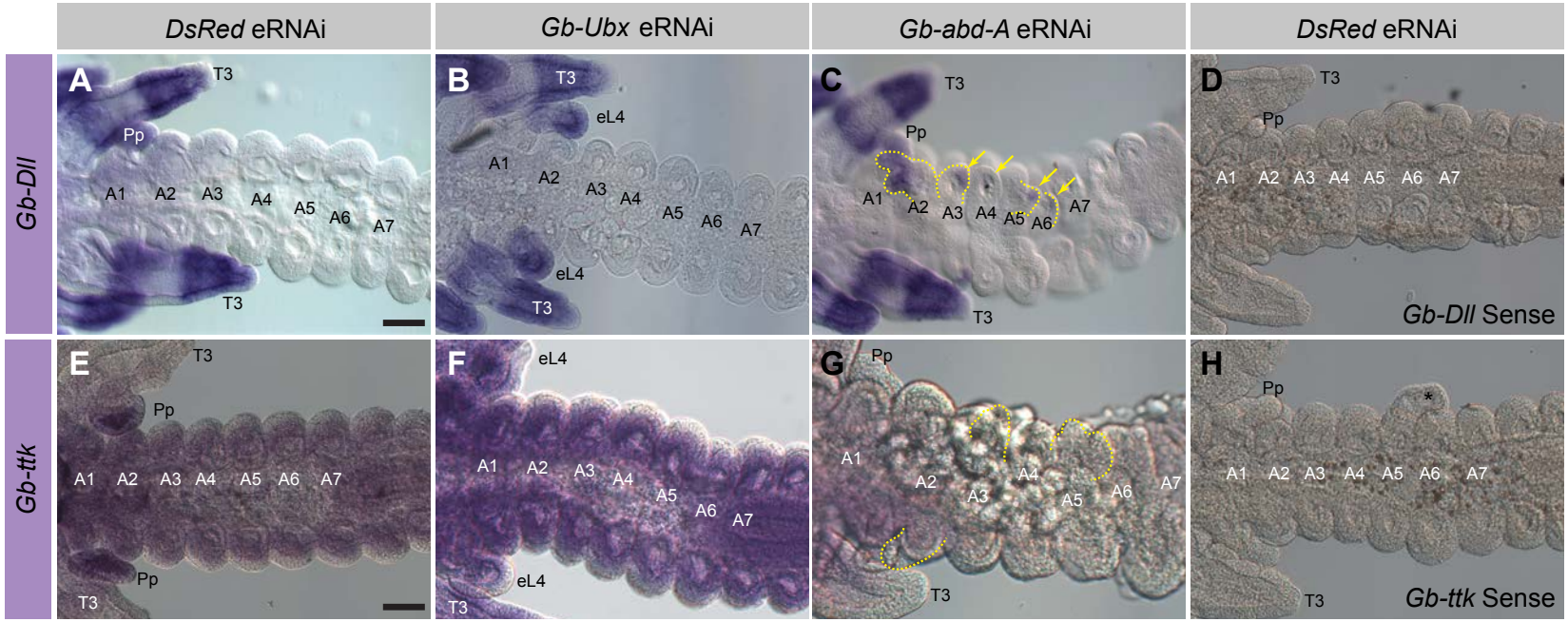

Fig. S6. Expression patterns of *G. bimaculatus Distal-less* (*Gb-Dll*) and *tramtrack* (*Gb-ttk*) in *Gb-Ubx* and *Gb-abdominal-A* eRNAi embryos. (A-D) *In situ* hybridization for *Gb-Dll* in Hox eRNAi embryos compared with *DsRed* eRNAi control. (A) *Gb-Dll* expression in wild type embryos is detectable in appendages; thoracic legs and pleuropodia (A1) are visible in the figure. (B) *Gb-Ubx* eRNAi embryo shows enlargement of A1 appendage with distally localized *Gb-Dll* expression in the transformed structure. (C) *Gb-abd-A* eRNAi embryo shows ectopic extrusions (marked by yellow dotted lines) in A2-A6 segments. Ectopic *Gb-Dll* expression is detected in these extrusions. (D) Sense RNA probe against *Gb-Dll* used as negative *in situ* control in *DsRed* embryos. (E-H) *In situ* hybridization for *Gb-ttk* in Hox eRNAi embryos compared with *DsRed* eRNAi control. (E) *Gb-ttk* transcripts are enriched in pleuropodia, and low-level expression is also detectable throughout the entire embryo in *DsRed* eRNAi controls. (F) *Gb-Ubx* eRNAi embryo shows reduced expression in pleuropodia and slightly increased expression in the rest of the abdomen. (G) In *Gb-abd-A* eRNAi embryos *Gb-ttk* expression are lost from ectopic abdominal extrusions and nearly entirely from the rest of the embryo. (H) Sense RNA probe against *Gb-ttk* used as negative *in situ* control in *DsRed* embryos. Ax: abdominal segment x; eL4: ectopic 4th leg; Pp: pleuropodia; T3: 3rd thoracic leg. Scale bar = 100 μm for all panels.

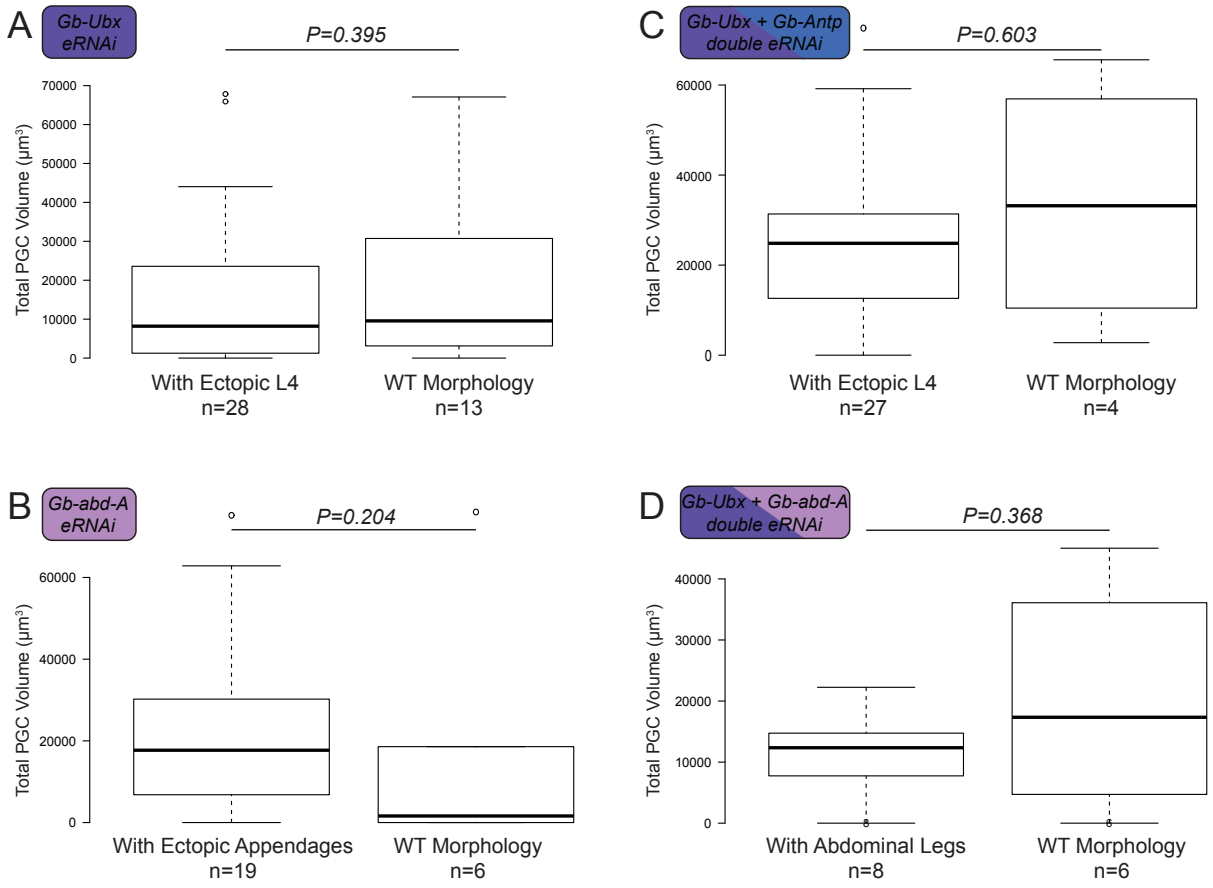

Fig. S7. **Statistical comparisons of PGC volumes from eRNAi embryos with and without homeotic phenotypes.** (A) *Gb-Ubx*, (B) *Gb-abd-A* (C) *Gb-Antp+Gb-Ubx* and (D) *Gb-Ubx+Gb-abd-A* eRNAi knockdowns. In each condition, the distributions of the total PGC numbers per embryo were not statistically different between embryos with homeotic phenotypes and those without. The whiskers extend to data points that are 1.5 times above the interquartile range away from the first or third quartile. The black lines represent the medians. n= the number of embryos observed for each condition. P-values for (A-C) were based on the Mann-Whitney Test, and the P-value for (D) is based on a t-test due to the low number of samples in this comparison.

Figure S8
Barnett, Nakamura & Extavour

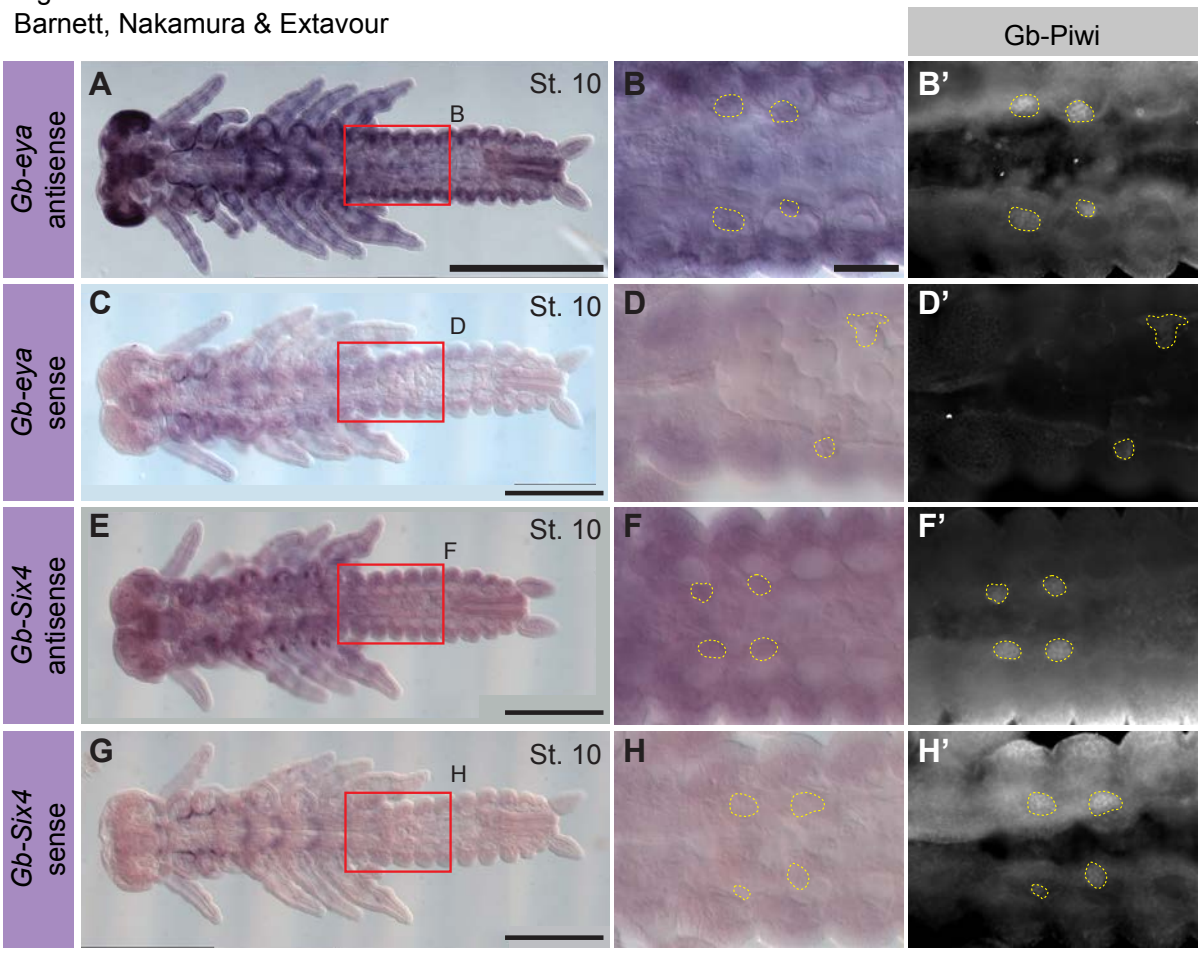

Fig. S8. Expression of *G. bimaculatus eyes-absent* (*Gb-eya*) and *Six4* (*Gb-Six4*) in PGC development. (A-D') *Gb-eya* transcripts are detectable at highest levels in the eye and brain primordia, and in the appendages in ring-like patterns. (B-B') High magnification view of the abdominal region boxed in red in (A) shows that *Gb-eya* is expressed in each abdominal coelomic pouch, but not obviously at high levels in or adjacent to PGCs (marked by yellow dotted lines and labeled with anti-Gb-Piwi (B')). (C, D) Sense RNA probe against *Gb-eya* was used as a negative *in situ* hybridization control. (E-H') *Gb-Six4* transcripts are detected throughout the entire embryo, with increased expression in the thoracic coelomic pouches. (F-F') High magnification view of the abdominal region boxed in red in (E) shows no enriched *Gb-Six-4* expression in or around PGCs. Scale bar = 500 μm in A, C, E, G and 100 μm in B, applicable to B-H'.

Table S1: Embryonic RNAi injection statistics.

Injectant	Concentration	# Embryos Injected	# (%) Embryos Survived Injection to Stage 8	# Embryos scored for PGCs in segments A1-A5
DsRed dsRNA	6 µg/µl	3,190	1,395 (43.7)	66
	9 µg/µl	417	176 (42.2)	16
Gb-Scr dsRNA	6 µg/µl	344	175 (50.9)	36
Gb-Antp dsRNA	6 µg/µl	1,103	251 (22.8)	14
Gb-Ubx dsRNA	6 µg/µl	203	163 (80.3)	29
	9 µg/µl	372	112 (30.1)	12
Gb-abd-A dsRNA	6 µg/µl	1,126	375 (33.3)	16
	8 µg/µl	149	22 (14.8)	9
Gb-Scr/abd-A RNAi	3 µg/µl each	268	0 (0)	0
Gb-Scr/Antp RNAi	3 µg/µl each	243	0 (0)	0
Gb-Antp/Ubx dsRNA	3 µg/µl each	374	201 (53.7)	31
Gb-Antp/abd-A dsRNA	3 µg/µl each	330	142 (43.0)	20
Gb-Ubx/abd-A dsRNA	3 µg/µl each	192	84 (43.8)	14

Table S2: Mann-Whitney U test statistics on PGC measurements for single eRNAi treatments. A1-5, abdominal segments 1-5.

Comparison	U Value	Z Score	P-Value	Significant?
Gb-Scr VS. DsRed A1	5858.5	-0.0931	0.9282	No
Gb-Scr VS. DsRed A2	3330.0	-5.3290	< .00001	Yes
Gb-Scr VS. DsRed A3	3714.5	-4.5328	< .00001	Yes
Gb-Scr VS. DsRed A4	4570.0	-2.7613	0.0057	Yes
Gb-Scr VS. DsRed A5	5730.0	-0.3592	0.7188	No
Gb-Scr VS. DsRed Total	691.0	-4.5851	< .00001	Yes
Gb-Antp VS. DsRed A1	1900.5	-1.4534	0.1470	No
Gb-Antp VS. DsRed A2	1316.0	-3.6042	0.0032	Yes
Gb-Antp VS. DsRed A3	1712.0	-2.1471	0.0315	Yes
Gb-Antp VS. DsRed A4	1900.5	-1.4534	0.1470	No
Gb-Antp VS. DsRed A5	2241.0	-0.2005	0.8414	No
Gb-Antp VS. DsRed Total	311.0	-2.7249	0.0065	Yes
Gb-Ubx VS. DsRed A1	6518.5	-0.0792	0.9362	No
Gb-Ubx VS. DsRed A2	6078.0	-1.2269	0.2187	No
Gb-Ubx VS. DsRed A3	6349.5	-0.7108	0.4777	No
Gb-Ubx VS. DsRed A4	6299.0	-0.8068	0.4179	No
Gb-Ubx VS. DsRed A5	6553.0	-0.0893	0.9282	No
Gb-Ubx VS. DsRed Total	1513.0	-0.8986	0.3681	No
Gb-abd-A VS. DsRed A1	3962.0	-0.3587	0.7188	No
Gb-abd-A VS. DsRed A2	3325.0	-2.0206	0.0433	Yes
Gb-abd-A VS. DsRed A3	3450.0	-1.6945	0.0910	No
Gb-abd-A VS. DsRed A4	3839.0	-0.6796	0.4965	No
Gb-abd-A VS. DsRed A5	3988.0	-0.2909	0.7718	No
Gb-abd-A VS. DsRed Total	818.0	-1.5202	0.1285	No

Table S3: Mann-Whitney U test statistics on PGC measurements for double eRNAi treatments. A1-5, abdominal segments 1-5.

Comparison	U Value	Z Score	P-Value	Significant?
(Gb-Antp+Gb-Ubx) VS. DsRed A1	5033.5	-0.1140	0.9124	No
(Gb-Antp+Gb-Ubx) VS. DsRed A2	2820.0	-5.1610	< .00001	Yes
(Gb-Antp+Gb-Ubx) VS. DsRed A3	3756.0	-3.0268	0.0024	Yes
(Gb-Antp+ Gb-Ubx) VS. DsRed A4	3331.5	-3.9947	0.0001	Yes
(Gb-Antp+ Gb-Ubx) VS. DsRed A5	4734.0	-0.7969	0.4237	No
(Gb-Antp+ Gb-Ubx) VS. DsRed Total	660.0	-3.9285	0.0001	Yes
(Gb-Ubx+ Gb-abd-A) VS. DsRed A1	2282.0	0.0496	0.9601	No
(Gb-Ubx+ Gb-abd-A) VS. DsRed A2	2204.0	-0.3366	0.7279	No
(Gb-Ubx+ Gb-abd-A) VS. DsRed A3	1755.0	-1.9888	0.0466	Yes
(Gb-Ubx+ Gb-abd-A) VS. DsRed A4	1598.5	-2.5647	0.0105	Yes
(Gb-Ubx+ Gb-abd-A) VS. DsRed A5	2243.0	-0.1931	0.8493	No
(Gb-Ubx+ Gb-abd-A) VS. DsRed Total	492.0	-0.8460	0.3953	No
(Gb-Antp+ Gb-abd-A) VS. DsRed A1	3054.5	-0.6721	0.5029	No
(Gb-Antp+ Gb-abd-A) VS. DsRed A2	2928.5	-1.0485	0.2937	No
(Gb-Antp+ Gb-abd-A) VS. DsRed A3	1319.0	-5.8563	< .00001	Yes
(Gb-Antp+ Gb-abd-A) VS. DsRed A4	2040.0	-3.7026	0.0002	Yes
(Gb-Antp+ Gb-abd-A) VS. DsRed A5	2744.0	-1.5996	0.1096	No
(Gb-Antp+ Gb-abd-A) VS. DsRed A6	3116.0	-0.4884	0.6241	No
(Gb-Antp+ Gb-abd-A) VS. DsRed Total	224.0	-5.0191	< .00001	Yes

Table S4: Statistical tests of presence/absence of PGC clusters in single Hox eRNAi treatments. FE = Fisher's Exact Test; X2 = Chi-Square Test; N/A = not applicable; A1-5, abdominal segments 1-5.

Comparison	Test	X2 Statistic	P-Value	Significant?
Gb-Scr VS. DsRed A1	FE	N/A	0.518	No
Gb-Scr VS. DsRed A2	X2	26.976	< .00001	Yes
Gb-Scr VS. DsRed A3	X2	25.818	< .00001	Yes
Gb-Scr VS. DsRed A4	X2	18.832	0.000	Yes
Gb-Scr VS. DsRed A5	FE	N/A	0.168	No
Gb-Antp VS. DsRed A1	FE	N/A	0.000	Yes
Gb-Antp VS. DsRed A2	X2	18.585	0.000	Yes
Gb-Antp VS. DsRed A3	X2	9.269	0.002	Yes
Gb-Antp VS. DsRed A4	X2	6.784	0.009	Yes
Gb-Antp VS. DsRed A5	FE	N/A	0.271	No
Gb-Ubx VS. DsRed A1	FE	N/A	1.000	No
Gb-Ubx VS. DsRed A2	X2	0.945	0.331	No
Gb-Ubx VS. DsRed A3	X2	1.604	0.205	No
Gb-Ubx VS. DsRed A4	X2	1.924	0.165	No
Gb-Ubx VS. DsRed A5	FE	N/A	0.602	No
Gb-abd-A VS. DsRed A1	FE	N/A	0.137	No
Gb-abd-A VS. DsRed A2	FE	N/A	0.059	No
Gb-abd-A VS. DsRed A3	X2	4.362	0.037	Yes
Gb-abd-A VS. DsRed A4	X2	1.601	0.206	No
Gb-abd-A VS. DsRed A5	FE	N/A	0.137	No

Table S5: Statistical tests of presence/absence of PGC clusters in double Hox eRNAi treatments. FE = Fisher's Exact Test; X2 = Chi-Square Test; N/A = not applicable; A1-6, abdominal segments 1-6.

Comparison	Test	X2 Statistic	P-Value	Significant?
(Gb-Antp+ Gb-Ubx) VS. DsRed A1	FE	N/A	0.4743	No
(Gb-Antp+ Gb-Ubx) VS. DsRed A2	X2	30.0584	< .00001	Yes
(Gb-Antp+ Gb-Ubx) VS. DsRed A3	X2	9.7186	0.0018	Yes
(Gb-Antp+ Gb-Ubx) VS. DsRed A4	X2	35.1369	< .00001	Yes
(Gb-Antp+ Gb-Ubx) VS. DsRed A5	FE	N/A	0.0065	Yes
(Gb-Ubx+ Gb-abd-A) VS. DsRed A1	FE	N/A	1.0000	No
(Gb-Ubx+ Gb-abd-A) VS. DsRed A2	X2	0.4714	0.4923	No
(Gb-Ubx+ Gb-abd-A) VS. DsRed A3	FE	N/A	0.0007	Yes
(Gb-Ubx+ Gb-abd-A) VS. DsRed A4	X2	18.5549	0.0000	Yes
(Gb-Ubx+ Gb-abd-A) VS. DsRed A5	FE	N/A	0.2710	No
(Gb-Antp+ Gb-abd-A) VS. DsRed A1	FE	N/A	0.0244	Yes
(Gb-Antp+ Gb-abd-A) VS. DsRed A2	X2	11.2953	0.0008	Yes
(Gb-Antp+ Gb-abd-A) VS. DsRed A3	X2	25.6402	< .00001	Yes
(Gb-Antp+ Gb-abd-A) VS. DsRed A4	X2	24.5565	< .00001	Yes
(Gb-Antp+ Gb-abd-A) VS. DsRed A5	FE	N/A	0.0000	Yes
(Gb-Antp+ Gb-abd-A) VS. DsRed A6	FE	N/A	0.0000	Yes

Table S6: Mann-Whitney U test statistics on PGC measurements for single vs. double eRNAi treatments. A1-6, abdominal segments 1-6.

Comparison	U Value	Z Score	P-Value	Significant?
(Gb-Antp+ Gb-Ubx) VS. Gb-Antp A1	759.0	-1.18816	0.234	No
(Gb-Antp+ Gb-Ubx) VS. Gb-Antp A2	811.0	0.49243	0.624	No
(Gb-Antp+ Gb-Ubx) VS. Gb-Antp A3	834.0	0.29197	0.772	No
(Gb-Antp+ Gb-Ubx) VS. Gb-Antp A4	709.5	1.37706	0.168	No
(Gb-Antp+ Gb-Ubx) VS. Gb-Antp A5	829.5	0.33119	0.741	No
(Gb-Antp+ Gb-Ubx) VS. Gb-Antp Total	194.0	0.55163	0.582	No
(Gb-Antp+ Gb-Ubx) VS. Gb-Ubx A1	2470.5	-0.03702	0.968	No
(Gb-Antp+ Gb-Ubx) VS. Gb-Ubx A2	1764.5	-3.13491	0.002	Yes
(Gb-Antp+ Gb-Ubx) VS. Gb-Ubx A3	1997.5	-2.19484	0.028	Yes
(Gb-Antp+ Gb-Ubx) VS. Gb-Ubx A4	1824.5	-2.89283	0.004	Yes
(Gb-Antp+ Gb-Ubx) VS. Gb-Ubx A5	2339.0	-0.57791	0.562	No
(Gb-Antp+ Gb-Ubx) VS. Gb-Ubx Total	399.0	-2.68391	0.007	Yes
(Gb-Ubx+ Gb-abd-A) VS. Gb-Ubx A1	1106.0	0.09464	0.928	No
(Gb-Ubx+ Gb-abd-A) VS. Gb-Ubx A2	1063.0	0.57983	0.562	No
(Gb-Ubx+ Gb-abd-A) VS. Gb-Ubx A3	944.0	-1.39639	0.162	No
(Gb-Ubx+ Gb-abd-A) VS. Gb-Ubx A4	864.0	-1.94534	0.0511	Approaching
(Gb-Ubx+ Gb-abd-A) VS. Gb-Ubx A5	1109.0	-0.07361	0.944	No
(Gb-Ubx+ Gb-abd-A) VS. Gb-Ubx Total	258.0	-0.55066	0.582	No
(Gb-Ubx+ Gb-abd-A) VS. Gb-abd-A A1	672.0	0.28645	0.772	No
(Gb-Ubx+ Gb-abd-A) VS. Gb-abd-A A2	586.0	1.18225	0.238	No
(Gb-Ubx+ Gb-abd-A) VS. Gb-abd-A A3	658.5	-0.42707	0.667	No
(Gb-Ubx+ Gb-abd-A) VS. Gb- abd-A A4	531.0	-1.75514	0.078	No
(Gb-Ubx+ Gb-abd-A) VS. Gb-abd-A A5	697.0	0.02604	0.976	No
(Gb-Ubx+abd-A) VS. Gb-abd-A Total	163.0	0.33669	0.728	No
(Gb-abd-A+ Gb-Antp) VS. Gb-abd-A A1	610.5	0.32864	0.741	No
(Gb-abd-A+ Gb-Antp) VS. Gb-abd-A A2	891.0	0.88102	0.379	No
(Gb-abd-A+ Gb-Antp) VS. Gb-abd-A A3	518.0	-3.90977	0.000	Yes
(Gb-abd-A+ Gb-Antp) VS. Gb-abd-A A4	661.0	-2.74861	0.006	Yes
(Gb-abd-A+ Gb-Antp) VS. Gb- abd-A A5	858.0	-1.14898	0.250	No
(Gb-abd-A+ Gb-Antp) VS. Gb-abd-A A6	950.0	-0.40194	0.689	No
(Gb-abd-A+ Gb-Antp) VS. Gb- abd-A Total	115.0	-3.0722	0.002	Yes
(Gb-abd-A+ Gb-Antp) VS. Gb-Antp A1	523.0	-0.68685	0.490	No
(Gb-abd-A+ Gb-Antp) VS. Gb-Antp A2	366.0	-2.41123	0.016	Yes
(Gb-abd-A+ Gb-Antp) VS. Gb-Antp A3	305.0	3.17135	0.001	Yes
(Gb-abd-A+ Gb-Antp) VS. Gb-Antp A4	412.0	1.82555	0.067	No
(Gb-abd-A+ Gb-Antp) VS. Gb-Antp A5	483.5	0.94705	0.342	No
(Gb-abd-A+ Gb-Antp) VS. Gb-Antp A6	532.0	0.34268	0.728	No
(Gb-abd-A+ Gb-Antp) VS. Gb-Antp Total	69.0	2.46699	0.013	Yes
Gb-Antp VS. Gb-Ubx Total	177.0	-2.1157	0.034	Yes

Gb-Antp VS. Gb-abd-A Total	140.0	-1.01006	0.312	No
Gb-Ubx VS. Gb- abd-A Total	461.0	-0.67416	0.503	No

Table S7: Statistical tests of presence/absence of PGC clusters in single vs. double Hox eRNAi treatments. FE = Fisher's Exact Test; X2 = Chi-Square Test; NA = not applicable.

Comparison	Test	X2 Statistic	P-Value	Significant?
(Gb-Antp+Gb-Ubx) VS. Antp A1	FE	N/A	0.0103	Yes
(Gb-Antp+Gb-Ubx) VS. Antp A2	X2	0.0395	0.8424	No
(Gb-Antp+Gb-Ubx) VS. Antp A3	X2	0.6814	0.4091	No
(Gb-Antp+Gb-Ubx) VS. Antp A4	X2	2.4911	0.1144	No
(Gb-Antp+Gb-Ubx) VS. Antp A5	FE	N/A	1.0000	No
(Gb-Antp+Gb-Ubx) VS. Ubx A1	FE	N/A	1.0000	No
(Gb-Antp+Gb-Ubx) VS. Ubx A2	X2	22.8716	< .00001	Yes
(Gb-Antp+Gb-Ubx) VS. Ubx A3	X2	3.6863	0.0548	No
(Gb-Antp+Gb-Ubx) VS. Ubx A4	X2	15.5755	0.0000	Yes
(Gb-Antp+Gb-Ubx) VS. Ubx A5	FE	N/A	0.2398	No
(Gb-Ubx+Gb-abd-A) VS. Ubx A1	FE	N/A	1.0000	No
(Gb-Ubx+Gb-abd-A) VS. Ubx A2	X2	0.0355	0.8504	No
(Gb-Ubx+Gb-abd-A) VS. Ubx A3	X2	6.6956	0.0096	Yes
(Gb-Ubx+Gb-abd-A) VS. Ubx A4	X2	8.2739	0.0040	Yes
(Gb-Ubx+Gb-abd-A) VS. Ubx A5	FE	N/A	1.0000	No
(Gb-Ubx+Gb-abd-A) VS. abd-A A1	FE	N/A	0.5338	No
(Gb-Ubx+Gb-abd-A) VS. abd-A A2	X2	0.5093	0.4754	No
(Gb-Ubx+Gb-abd-A) VS. abd-A A3	X2	2.954	0.0856	No
(Gb-Ubx+Gb-abd-A) VS. abd-A A4	X2	6.0295	0.0140	Yes
(Gb-Ubx+Gb-abd-A) VS. abd-A A5	FE	N/A	1.0000	No
(Gb-Antp+Gb-abd-A) VS. Antp A1	FE	N/A	0.2589	No
(Gb-Antp+Gb-abd-A) VS. Antp A2	X2	5.5567	0.0184	Yes
(Gb-Antp+Gb-abd-A) VS. Antp A3	FE	N/A	0.1150	No
(Gb-Antp+Gb-abd-A) VS. Antp A4	X2	2.7686	0.0961	No
(Gb-Antp+Gb-abd-A) VS. Antp A5	FE	N/A	0.0706	No
(Gb-Antp+Gb-abd-A) VS. Antp A6	FE	N/A	0.0000	Yes
(Gb-Antp+Gb-abd-A) VS. abd-A A1	FE	N/A	0.6521	No
(Gb-Antp+Gb-abd-A) VS. abd-A A2	X2	0.0204	0.8865	No
(Gb-Antp+Gb-abd-A) VS. abd-A A3	FE	N/A	0.0013	Yes
(Gb-Antp+Gb-abd-A) VS. abd-A A4	X2	10.395	0.0012	Yes
(Gb-Antp+Gb-abd-A) VS. abd-A A5	FE	N/A	0.0208	Yes
(Gb-Antp+Gb-abd-A) VS. abd-A A6	FE	N/A	0.0000	Yes

Table S8: Primers used for gene cloning and qPCR.

Gene name / primer name	Gene region targeted	length (bp)	Forward primers (5'-3')	Reverse primers (5'-3')
Gb-Scr, qPCR	ORF	91	AAGAAGGAGCACAAGATGGC	AGGGCCGCATTTTTACAGTG
Gb-Antp, qPCR	ORF	136	GCGCATGAAGTGGAAGAAAGAG	GCTATAAATTAGGGGCGTGTGG
Gb-Ubx, qPCR	ORF	117	AGCGATCAAAGAGCTCAACG	AGGAAACTCGACTCTTCTCGAC
Gb-abd-A, qPCR	ORF	121	TTCTCAAGGCAGTGGCAAAG	TGAACGCAGATGAGGCATTG
Gb-eya	ORF	950	AGGGACAGTGCTTGTGAAGG	ACACACGAGTCAATCACTGG
Gb-six4	ORF	321	CTGTACAGCATCCTGGAGGG	GAACCAGTTGCTGACTTGCG

SI References

1. Horch HW, Mito T, Popadic A, Ohuchi H, & Noji S eds (2017) *The Cricket as a Model Organism: Development, Regeneration and Behaviour* (Springer), p 376.
2. Ewen-Campen B, Donoughe S, Clarke DN, & Extavour CG (2013) Germ cell specification requires zygotic mechanisms rather than germ plasm in a basally branching insect. *Curr. Biol.* 23(10):835-842.
3. Donoughe S*, et al.* (2014) BMP signaling is required for the generation of primordial germ cells in an insect. *Proc. Natl. Acad. Sci. USA* 111(11):4133-4138.
4. Pavlopoulos A*, et al.* (2009) Probing the evolution of appendage specialization by Hox gene misexpression in an emerging model crustacean. *Proc. Natl. Acad. Sci. USA* 106(33):13897-13902.
5. Singh NP & Mishra RK (2014) Role of abd-A and Abd-B in development of abdominal epithelia breaks posterior prevalence rule. *PLoS Genet* 10(10):e1004717.
6. Pelaz S, Urquia N, & Morata G (1993) Normal and ectopic domains of the homeotic gene Sex combs reduced of Drosophila. *Development* 117(3):917-923.
7. Andrew DJ, Horner MA, Petitt MG, Smolik SM, & Scott MP (1994) Setting limits on homeotic gene function: restraint of Sex combs reduced activity by teashirt and other homeotic genes. *EMBO J.* 13(5):1132-1144.
8. Little JW, Byrd CA, & Brower DL (1990) Effect of abx, bx and pbx mutations on expression of homeotic genes in Drosophila larvae. *Genetics* 124(4):899-908.
9. Struhl G (1982) Genes controlling segmental specification in the Drosophila thorax. *Proc Natl Acad Sci U S A* 79(23):7380-7384.
10. Edgar RC (2004) MUSCLE: a multiple sequence alignment method with reduced time and space complexity. *BMC Bioinformatics* 5:113.
11. Lefort V, Longueville JE, & Gascuel O (2017) SMS: Smart Model Selection in PhyML. *Mol. Biol. Evol.* 34(9):2422-2424.
12. Guindon S & Gascuel O (2003) A simple, fast, and accurate algorithm to estimate large phylogenies by maximum likelihood. *Syst. Biol.* 52(5):696-704.
13. Kainz F, Ewen-Campen B, Akam M, & Extavour CG (2011) Delta/Notch signalling is not required for segment generation in the basally branching insect *Gryllus bimaculatus*. *Development* 138(22):5015-5026.
14. Donoughe S & Extavour CG (2016) Embryonic development of the cricket *Gryllus bimaculatus*. *Dev. Biol.* 411(1):140-156.